CERN 77-08
Proton Synchrotron
Division
13 April, 1977

ORGANISATION EUROPÉENNE POUR LA RECHERCHE NUCLÉAIRE
CERN EUROPEAN ORGANIZATION FOR NUCLEAR RESEARCH

STUDIES ON ELECTRON COOLING OF HEAVY PARTICLE BEAMS MADE BY THE VAPP-NAP GROUP AT THE NUCLEAR PHYSICS INSTITUTE OF THE SIBERIAN BRANCH OF THE USSR ACADEMY OF SCIENCE AT NOVOSIBIRSK*

PART A

Review of theoretical and experimental studies

PART B

The electron beam device for heavy particle cooling experiments

PART C

Bibliography

G E N E V A

1977

* Extended version of the Seminar report given at CERN on 24th March, 1977.

CERN - Service d'information scientifique - RD/230 - 2000 - avril 1977

SUMMARY

This report consists of three parts: the first one is a summary report of electron cooling studies, both theoretical and experimental, which were performed during the years 1966-1976. The second part, which describes the electron beam device for the electron cooling experiments, is the translation of a Novosibirsk preprint. Finally, a bibliography of papers on electron cooling and related problems is given in part three.

FOREWORD AND ACKNOWLEDGEMENTS

The purpose of this report is to give a review of theoretical and experimental results, which emerged during 10 years of electron cooling studies. The report is based on the work carried out at the Institute of Nuclear Physics,Novosibirsk, by G. Budker, Y. Derbenev, N. Dikansky, I. Meshkov, V. Parkhomchuk, D. Pestrikov, R. Salimov, A. Skrinsky, B. Sukhina and colleagues. Our aim is to pass on to the people - at CERN and elsewhere - who are starting to apply electron cooling methods, all the principles and details which turned out to be important in the construction of, and the experimentation with, our cooling device. At the same time, we would like to discuss some recent theoretical work which, we think, may be relevant to the interpretation of the experiments.

The initiative for preparing this publication belongs to the Initial Cooling Experiment (ICE) Group at CERN, and we would like to thank them for their assistance and hospitality. Special thanks are due to O. Barbalat, D. Möhl and K.H. Reich. It is due to their effective help that we are able to issue this report in English.

We would also like to thank the CERN Management for providing the framework for our - as we hope - successful work at CERN.

Finally, thanks are due to Mrs.Durieu and Miss Innocenti who undertook the difficult task to type this report at rather short notice.

Y. Derbenev

I. Meshkov

CERN, March 1977

PART A

REVIEW OF THEORETICAL AND EXPERIMENTAL STUDIES ON ELECTRON COOLING

TABLE I - Some dates of the history of electron cooling
(First ten years at INP, Novosibirsk)

1966	First report by G. Budker (Saclay Symposium)
1966	First proton antiproton colliding beam proposal using electron cooling (G. Budker, A. Skrinsky, Saclay Symposium)
1967-70	Experimental study on the electron beam (I. Meshkov, R. Salimov, A. Skrinsky)
1968	Theoretical study of the kinetics of electron cooling (Y. Derbenev, A. Skrinsky)
1970	First $p\bar{p}$-project (VAPP-NAP-Group)
1972	Beginning of NAP-M design (N. Dikansky, D. Pestrikov, A. Skrinsky)
1974	The first successful electron cooling experiments (G. Budker, N. Dikansky, I. Meshkov, V. Parkhomchuk, D. Pestrikov, B. Sukhina, A. Skrinsky)
1976-77	Observation and study of the "fast" cooling
1976-77	Theory of "magnetized" electron beams with "flattened" distribution (Y. Derbenev, A. Skrinsky) (A possible explanation of the "fast" cooling)
1976	$p\bar{p}$-colliding beams projects (Novosibirsk for Serpukhov, Batavia, CERN).

§ 1. THE MAIN STAGES OF THE WORK ON ELECTRON COOLING

As electron cooling was recently demonstrated experimentally and the basic theory is now established, a brief historical review is in order (see Table I). The electron cooling method was suggested by G.I. Budker, and a first report was given by him at the 1966 International Symposium on Electron and Positron Storage Rings in Saclay [see Ref. I-1]. Similar ideas were examined by L. Spitzer and G. O'Neil at about the same time, but they did not publish their work. The first experiments to set up electron beams for cooling of heavy particles started in 1967 at the Institute for Nuclear Physics (INP) at Novosibirsk. These experiments were concerned with questions like gun optics [II-2,4,5] and electron beam control [II-7]. The theory of electron cooling was further developed at the same time [I-2]. The first proton-antiproton colliding beams project was published by the INP "Cooling group" (VAPP-NAP group) in 1970 [I-3]. The electron beam device was finished in 1970 [II-2,4] but, unfortunately, the opportunity for the construction of the experimental electron cooling ring only arose in 1972, starting date of the design and the construction of the proton storage ring NAP-M [III-1-5]. The first experiments were made during 1974. They immediately gave very successful results as reported in Ref. [I-3]. These experiments were continued during 1975-1976 and a new series of investigations is presently under way. We think our experiments have shown that the electron cooling method is a very effective tool [I-4,5,6,7] to obtain dense particle beams which can be used in many applications [I-5, 8-11].

§ 2. THE EXPERIMENTAL APPARATUS

The experimental study of electron cooling was performed on the proton storage ring NAP-M (abbreviation of the Russian words for "Antiproton Storage Ring Model"). The main parameters are given in Table II, the detailed description can be found in the reports [I-6, III-1-5]. The description of the electron-beam device, which is used in all experiments is given in Part B of this report and in the Articles [I-6, II-4]. The parameters are also given in Table II.

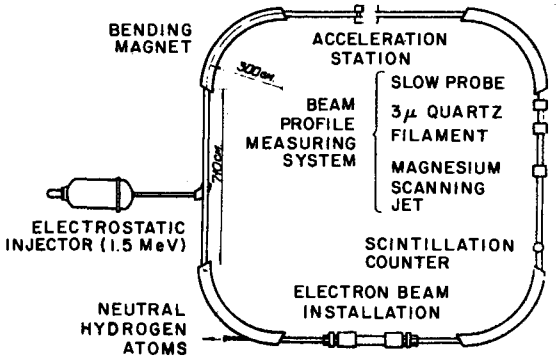

FIG. 1 - Layout of the proton accelerator NAP-M.

The proton beam diagnostics apparatus (Table III) is described in detail in Ref. [I-6]. Some recent changes and new experimental techniques are to be noted. The first one concerns the measurement of the longitudinal friction force, for which the magnesium jet is used; in these measurements the jet is located outside of the proton beam and the time of proton beam displacement onto the jet due to fast energy exchange with the electrons is registered. Previously, an aperture probe [I-6] was used for this, rather than the magnesium jet. Secondly we now measure the proton velocity spread, as to be described later (§ 7).

TABLE II - Main parameters of NAP-M
(AntiProton Storage Ring-Model)

Proton energy	up to 150 MeV
Injection energy	1.5 MeV
Curvature radius in magnets	3 m
Straight section length	7.1 m
Vacuum chamber apertures in magnets	
- vertical	± 3.5 cm
- radial	± 5 cm
Cooling section aperture	± 3.5 cm
β-function	
- at the ends of the straight sections	7.5 m
- in the cooling section	5.2 m
Momentum compaction function in straight sections	6 m
Transition energy	≈ 110 MeV
Duration of acceleration cycle	30 sec
Average pressure	5.10^{-10} Torr

Parameters of the electron beam device

Cooling section length	1 m
Electron energy	up to 100 kV
Electron current	up to 1 A
Longitudinal magnetic field	1 kG
Recovering efficiency ΔI/I	$10^{-4} \div 5.10^{-5}$
Collector potential V_{col}	1.5 kV

TABLE III - Proton Beam Diagnostics Apparatus

A. Measurement of proton current and position of proton beam

1. Luminescent screens (retractable)
2. Pick-up electrodes (electrostatic)
3. Beam current monitor

B. Profile analyzers

1. Slow-moving probes + scintillation counter (destructive method) resolution: $\Delta a \sim 0.1$ mm
2. Fast moving quartz filament + scintillation counter velocity: 5m/sec, thickness: $1 \div 2\ \mu$, resolution: 0.1 mm.
3. Thin scanning magnesium jet: $\Delta a \sim 0.5$ mm
4. H^o-method
   relation between beam (x_p) and H^o (x_{H^o}) dimensions:

$$\overline{x^2_{H^o}} \sim (1 + \frac{L^2}{\beta^2}\ \overline{x^2_p})$$

   L : distance from cooling region to H^o detector
   β : amplitude function in cooling region

C. Damping time measurements

Thin magnesium jet + deflector

D. Longitudinal friction force measurements

Thin magnesium jet + "energy jump".

TABLE IV - Experimental parameters and results

	1974	1975-1976
Electron current I_e	0.1 ÷ 0.25 A	0.1 ÷ 0.8 A
Electron current density j_e	0.13 ÷ 0.33 A/cm^2	0.13 ÷ 1.1 A/cm^2
Damping time τ_e (for J_e = 0.13 A/cm^2)	5 sec	0.4 sec ($\tau_{e\ min} \simeq$ 80 msec, I_e = 0.8 A)
Equilibrium dimension of proton beam (diameter) $2 \times \sqrt{\overline{x_p^2}}$	0.8 mm	0.47 mm
Effective electron temperature T_e	$\sim$ 0.2 eV	0.25 eV
Power of longitudinal friction force	-	0.5 MeV/sec for J_e = 0.13 A/cm^2
Momentum spread of proton beam $\Delta p/p$	-	$1.10^{-6} \div 1.10^{-5}$ for J_e = 0.13 A/cm^2 $\Delta p/p \propto I_p$
Flux of neutral hydrogen atoms $I_e^{-1}\ I_p^{-1}(dN/dt)$	17 A^{-1} μA^{-1} sec^{-1}	80 A^{-1} μA^{-1} sec^{-1}

§ 3. THE EXPERIMENTAL PARAMETERS AND RESULTS

Table IV gives a summary of experimental results, from the first experiments (1974) up to now (March 1977). These results are published in the papers [I-4,5,6,7].

Our experimental studies can be subdivided into two different periods: in the first period, the cooling time, achieved with an electron current density $j_e \simeq 0.13$ A/cm^2, was about 5 sec [I-4,5,6]. In the second period, the cooling time (for the same current density) was reduced to 0.4 sec [I-7]. The explanation of this "fast cooling" relates to effects of "flattened" distributions and "magnetized electron beams" (see below).

§ 4. THE "FLATTENED" DISTRIBUTION

This effect is connected with the deformation of the electron velocity distribution due to acceleration in the electric field of the gun. If the electron flux near the cathode has some effective temperature (given by the cathode temperature plus cathode potential fluctuations, etc.)

$$T_{eff} = T_{cathode} + e\Delta V_{\sim} \quad , \tag{1}$$

the electron energy after acceleration with a time-average voltage V_0 will be:

$$W = eV_0 + T_{eff} \equiv \frac{m}{2}(v_0 + \Delta)^2, \qquad (\gamma - 1)mc^2 = T_{eff} + eV_0. \tag{2}$$

with m the electron mass.

Here and later, we write on the left side the non-relativistic equations, and on the right the relativistic ones. The longitudinal velocity spread in the laboratory frame is

$$\Delta_{//} \simeq \frac{T_{eff}}{mv} \quad , \qquad \Delta_{//} \simeq \frac{T_{eff}}{\beta\gamma^3 mc} \quad , \tag{3}$$

In the particle rest frame (moving with the average electron velocity $v_0 \equiv \beta c$), these parameters are described by

$$\Delta'_{//} = \Delta_{//}, \qquad \Delta'_{//} \simeq \gamma^2 \Delta_{//} \quad , \tag{4}$$

and the effective "longitudinal temperature" of the electrons in the particle rest frame is:

$$T_{//} \equiv \frac{m(\Delta'_{//})^2}{2} = \frac{T_{eff}^2}{4W} \quad , \qquad T_{//} = \frac{T_{eff}^2}{2\beta^2\gamma^2 mc^2} \quad . \tag{5}$$

V. Parkhomchuk drew attention to the importance of this effect for electron cooling. It is easy to see that a situation can occur where in the particle rest frame $T_{//} << T_{\perp} \sim T_{eff}$. For example, for NAP-M parameters ($T_{cathode} \sim 0.1$ eV, $W \sim 40$ keV) we have $T_{//}/T_{\perp} \sim T_{cathode}/4W \sim 6.10^{-7}$.

This simple "flattened" situation can be destroyed due to electron-electron collisions in the electron beam. However, collision effects are negligible and expressions (5) are true if:

$$L_{cooler} >> \frac{v_0}{\omega_p} \quad , \tag{6}$$

where ω_p is the plasma frequency for the given electron beam density. In the opposite situation ($L_{cooler} \lesssim v_0/\omega_p$) the upper limit of longitudinal temperature can be estimated:

$$T_{//} > e^2 (n_e')^{1/3} = e^2 \left(\frac{j_e}{e\beta\gamma c}\right)^{1/3} \quad . \tag{7}$$

For NAP-M parameters we have:

$v_o/\omega_p \sim 20$ cm, $T_{//}$ (from eq. 5) $\sim 3.10^{-7}$ eV ($T_{eff} \sim 0.2$ eV),

$T_{//}$ (from eq. 7) $\sim 6.10^{-5}$ eV or $\Delta_{//}/\Delta_{\perp} \sim 2.10^{-2}$.

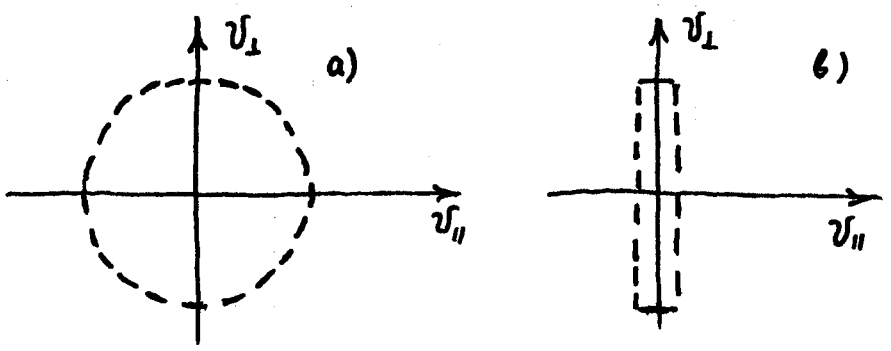

FIG. 2 : The particle density distribution in velocity space.
a) The uniform Maxwellian distribution
b) The "flattened" distribution.

The existence of the "flattened" distribution is proved by experiments on the longitudinal friction force F [I-6,7]. These measurements were being made with the help of a method in which after a small and fast change of the average electron velocity $\Delta_{/\!/}$, the displacement velocity dr/dt of the proton beam was measured:

$$\frac{dr}{dt} = \frac{\alpha\, R_s}{p_s}\, \eta\, F_{/\!/} \quad . \tag{8}$$

Here p_s is the proton momentum, $\alpha\, R_s$ the momentum compaction function, η the fraction of the circumference occupied by the electron beam. The dependence of $F_{/\!/}$ on $\Delta_{/\!/}$ agrees with the calculated function, if we choose [I-7]

$$T_\perp = 0.28 \pm 0.06 \text{ eV}, \qquad T_{/\!/} \ll T_e , \qquad L_p = 11 \quad ;$$

L_p here is the Coulomb logarithm for longitudinal momentum transfer in electron-proton collisions. If we modulate the electron energy ($\Delta V_\sim$ = 30 V, f = 500 Hz), the flatness of the distribution decreases in agreement with equation 3. Results of these measurements are displayed in Fig. 3.

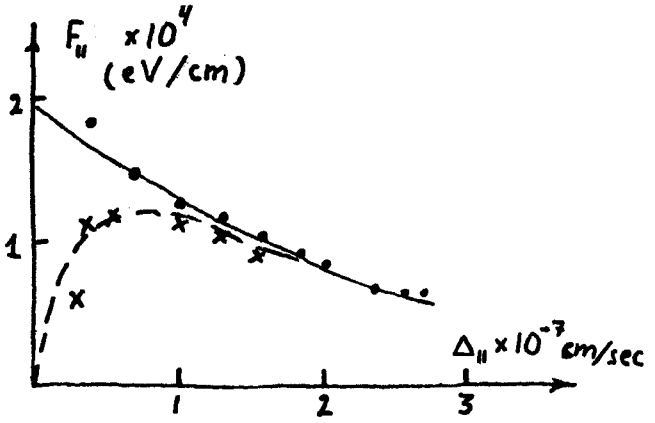

FIG. 3 : The longitudinal friction force as a function of fast-produced difference of average proton and electron velocities ($\Delta_{//}$).

————————	calculated curve
.....	experimental points
- x - x - x - x -	experimental curve for measurements with modulated electron energy.

It is necessary to note the steep dependence of the cooling time on the angle between electron and proton beam axes (Fig. 4). This effect was observed at the same time when fast cooling ("second period") was observed.

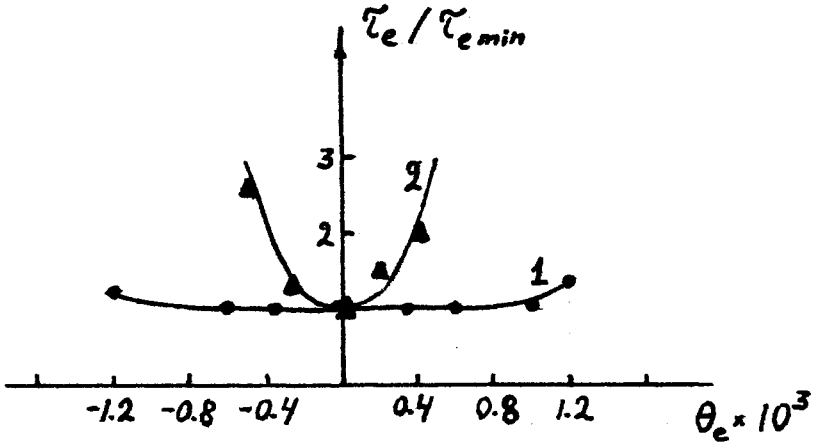

FIG. 4 : The dependence of damping time from angle between electron and proton beam axes.

1. The first period "slow damping"
2. The second period "fast damping".

§ 5. THE IMPLICATIONS OF THE THEORY OF THE "FLATTENED" DISTRIBUTION ON COOLING TIME

Using the electrostatic model for the friction force in the electron cooling process [I-2] we have

$$\vec{F} = -\frac{4\pi e^4 L_p n_e}{m} \int d^3V_e \frac{(\vec{v}_p - \vec{v}_e)}{|\vec{v}_p - \vec{v}_e|^3} f(\vec{v}_e) \quad . \tag{9}$$

Here, e, m, n_e are the charge, mass and the density of electrons, L_p is the Coulomb logarithm, $\vec{v}_e$, $\vec{v}_p$ the electron and proton velocities; all parameters are taken in the particle rest frame. It is now possible to calculate the damping time for the linear force region, provided that

$$v_p \ll v_{e\perp} \quad , \qquad \vec{F} \propto -\vec{v}_p \quad . \tag{10}$$

In this case the cooling time in the laboratory frame is

$$\tau_e = \frac{k}{\eta L_p r_p r_e} \frac{e}{j_e} \beta\gamma^3 \left(\frac{T_\perp}{mc^2}\right)^{3/2} \quad , \tag{11}$$

$$T_\perp = \beta^2\gamma^2 mc^2 \theta_e \quad , \qquad \theta_e = \frac{(v_e)_\perp}{v_0} \tag{12}$$

where j_e is the electron current density, r_e, r_p the classical radii of electron and proton. The numerical coefficient k is for

the uniform Maxwellian distribution	$k = \frac{3}{2\sqrt{2\pi}} = 0.6$,
the "flattened" distribution with constant density in velocity space ($T_{/\!/} \ll T_\perp$)	$k = \frac{1}{2\pi} = 0.16$.

In this way, the theory based on a flattened distribution can explain a decrease in cooling time by a factor 4.

A change of the experimental conditions between our first and second series of experiments has lead us to the situation where effects due to a "flattened" distribution began to manifest themselves. Such a change is, for example, the reduction of the electron energy fluctuations. In fact,

the gun voltage was stabilized to a high precision in our second series of experiments.

It is possible to estimate the (transverse) electron temperature from three independent parameters: the equilibrium dimension of the proton beam, the flux of neutral hydrogen atoms and the longitudinal friction force [I-7]. The results (Table V) agree with each other. But, if we calculate the electron

TABLE V - Estimates of effective electron temperature

Parameters	Value	Corresponding temperature ($T_\perp$)
Equilibrium dimension of the proton beam	0.47 mm	0.23 ± 0.07 eV
Flux of neutral hydrogen atoms	80 A^{-1} μA^{-1} sec^{-1}	0.24 ± 0.06 eV
Longitudinal friction force	(see Fig. 3)	0.28 ± 0.06 eV

temperature from the expression (10) for the cooling time, the result for the experimental data $\tau_e \cdot j_e = 64$ msec·A will be (k = 0.16) $T_\perp \simeq 0.06$ eV. This disagrees with the results of Table IV. It is certainly possible to find a distribution function $f(V_e)$, which leads to an even smaller value of the coefficient k and, thus to an agreement between $T_\perp \sim 0.2$ eV and the measured damping time. But this procedure is not convincing and a recent development of electron cooling theory reveals a strong enhancement of the cooling time which is connected with particularities of an electron beam in a longitudinal magnetic field.

§ 6. THE MAGNETIZED BEAM EFFECTS IN ELECTRON COOLING [I-14]

The kinetics of electron cooling has some pecularities, which distinguish it from the relaxation process of a two-component plasma. The difference is connected with the periodic character of the heavy particle motion in the storage ring, and with the conditions of the formation and the guidance of electron beam.

The early theory [I-1,2], which considered the general properties of electron cooling had established two important requirements on the electron beam parameters:

1. The angle $<\theta_e>$ between the axes of the electron beam and the heavy particle closed orbit in the cooling region has to be smaller than the velocity (θ_r) spread of the electrons:

$$<\theta_e> < \theta_T \quad . \tag{13}$$

If this condition is not satisfied, small proton oscillations increase due to collisions with electrons up to angular amplitudes

$$\theta_p \sim <\theta_e> \tag{14}$$

2. The transverse gradient in the longitudinal velocity of the electron has to be smaller than the average momentum compaction factor α_p of the protons:

$$\left|\frac{d(V_e)}{dr}\right| < \frac{d(V_p)}{dr} \equiv \alpha \frac{\beta c}{\gamma^2 R_s} \quad . \tag{15}$$

In the reverse case the cooling decrement in one of the two transverse directions - radial or vertical - will be negative.

A suitable electrostatic model was developed in the "old" theory; in particular relations for damping times for a uniform Maxwellian distribution [(11), k = 0.6] were obtained. The next step was concerned with "flattened" distributions, and after that the most recent refinement involves the "magnetized" electron beam theory. It should be noted that the kinetic equations for a plasma in a strong magnetic field were first obtained by S.T. Beljaev [IV-6]. However, the influence of a strong magnetic field on the electrons cooling process is negligible, if one has a uniform Maxwellian distribution of electron velocities. After the understanding of the effect of "flattened" distribution (V.V. Parkhomshuk, 1975) the time had come to study in detail

the effect of a "magnetized" beam; it is noted though that the general equations of the earlier papers [I-2] contain already a rough description of the electron beam situation in a strong longitudinal magnetic field.

Table VI contains the main equations describing the effects of a strong longitudinal magnetic field on the cooling process in the case of the "flattened" distribution.

The important property of the magnetized electron beam is the smallness of the Larmor radius for transverse electron velocities: $r_{Larmor} = \frac{\gamma m v_\perp c}{eH_0}$. In fact the Larmor radius in a typical cooling device is much smaller than the transverse dimensions of the electron beam a or the distance Δr, which the protons travel in the particle rest frame during the time of the transversal of the cooling region:

$$\Delta r = \left| \vec{v}_p' - (\vec{v}_e') \right| \frac{L_{cooler}}{v_0} \quad . \tag{16}$$

In this situation there is a large range of impact parameters ρ, leading to collisions between electrons and protons which are adiabatical in comparison with the Larmor period. This region of impact parameters is:

$$\rho_{min}^{A} \equiv \min \left\{ r_{Larmor} , \delta r \right\} < \rho < \max \left\{ a, \Delta r \right\} \equiv \rho_{max}^{A} \tag{17}$$

where

$$\delta r = \frac{e^2}{m \left| \vec{v}_p' - (\vec{v}_e') \right|^2} \tag{18}$$

is the distance at which the energy, given from a proton to an electron during a collision, is comparable to the kinetic energy of an electron moving at velocity $v_p - v_e$. If (17) is satisfied for the value of ρ, the proton transfers momentum to the electron only in the longitudinal direction. This means that for the region (17) the cooling interaction is only defined by the longitudinal velocity spread of the electrons. The Coulomb loga-

rithm for adiabatic collisions is:

$$L^A = \ln(\rho^A_{max}/\rho^A_{min}) \quad . \tag{19}$$

The results, given in Table VI, differ from the results of the earlier theory in at least one important aspect. The damping time formula does no longer contain the transverse electron temperature. The same is true for the equilibrium proton beam dimensions.

So far, an ideal longitudinal field was assumed. If the field strength varies periodically along the cooling section with a length of period large compared to the Larmor wavelength, then cooling time and equilibrium dimensions are determined by the average angular variation α_0 of the field-line.

There are other factors which may be important:

1. The drift of the Larmor motion of the electrons in the electric field of the electron beam;
2. The transverse gradient of electron Larmour radii due to aberrations of the gun optics;
3. The electron-electron interactions that lead to non-stationary shielding of the interaction between protons and electrons and, also, enhance the longitudinal temperature of the electron;
4. The coherent and non-coherent proton-proton interaction directly through the electron beam.

It is necessary to study in detail the influence of these and other factors in the next series of investigations. In addition, the theory must be improved by taking into consideration situations where relative longitudinal velocities are small so that the logarithmic (or adiabatical) approximation for magnetized electrons becomes poor.

TABLE VI

The effects of a magnetized electron beam with a "flattened" distribution in velocity space

A. The friction force for small proton velocities (particle rest frame)

$$\Delta_{/\!/} < v_p < \Delta_{\perp}$$

$$F^A_{\perp} = -\frac{8\pi n_e e^4}{m} L^A(v_p) \frac{v_{p\perp}^2 - 2v_{p/\!/}^2}{v_p^2} \frac{\vec{v}_{p\perp}}{v_p^3} ,$$

$$F^A_{/\!/} = -\frac{6\pi n_e e^4}{m} L^A(v_p) \frac{v_{p\perp}^2}{v_p^2} \frac{v_{p/\!/}}{v_p^3}$$

B. The minimum damping time (Lab. frame)

$$\tau_e = \frac{1}{\sqrt{2\pi}} \cdot \frac{1}{\eta L^A r_p r_e} \cdot \frac{e}{j_e} \beta\gamma^2 \left(\frac{T_{/\!/}}{mc^2}\right)^{3/2} , \quad v_{p/\!/} < \Delta_{/\!/}$$

[$T_{/\!/}$ - see formulae (5) and (6)].

C. The minimum equilibrium proton temperature

$$(T_p)_{min} \simeq T_{/\!/} \qquad \text{(particle rest frame)}$$

$$(\theta_p)_{min} \simeq \sqrt{\frac{m}{M}} \frac{T_{eff}}{\beta^2\gamma^2 mc^2} \qquad \text{(laboratory frame)}$$

D. The effect of curvature of magnetic field lines

$$\Delta_{\perp}/\gamma\beta c > \alpha_0 > \Delta_{/\!/}/\gamma\beta c$$

$$(\tau_{\perp})_{min} \simeq \left(\frac{2}{\pi}\right)^{3/2} \frac{1}{\eta L^A r_p r_e} \frac{e}{j_e} \beta\gamma^2 (\beta\gamma\alpha_0)^3$$

$$(\tau_{/\!/})_{min} \simeq \frac{\sqrt{\pi}}{4\sqrt{2}} \cdot \frac{v_{/\!/}}{\beta\gamma c\alpha_0} (\tau_{\perp})_{min}$$

$$(T_p)_{\perp} \simeq m(\beta\gamma c\alpha_0)^2 ; \quad (T_p)_{/\!/} \simeq \sqrt{(T_p)_{\perp} T_{/\!/}} \qquad \text{(particle rest frame)}$$

§ 7. THE MEASUREMENTS OF MOMENTUM SPREAD OF THE PROTON BEAM

The method used in these measurements was to create a short gap in the coasting proton beam, and to observe the time, during which this gap was refilled by the beam. Pick-up electrodes were used for these measurements.

If the gap is produced by a short reactangular inflector pulse of length τ, the pick-up signal can be written in spectral form as

$$V(t) = V_{amp} \int f(\omega) d\omega \sum \sin k\omega t \, \frac{\sin k\omega\tau}{k\omega\tau} \quad , \tag{20}$$

where V_{amp} is the signal amplitude, $f(\omega)$ the distribution function of proton revolution frequencies ω. Assuming that

$$f(\omega) = A \exp \left\{ - \frac{(\omega - \omega_0)^2}{2(\Delta\omega)^2} \right\} \quad , \tag{21}$$

it is easy to calculate that:

$$V(t) \; \alpha \; e^{-(\Delta\omega)^2 (t+\tau)^2/2} \quad . \tag{22}$$

Since the debunching time $\tau_{debunch}$ is much longer than the pulse duration τ, we can write:

$$\tau_{debunch} = \frac{\sqrt{2}}{\Delta\omega} \; ; \qquad \frac{\Delta\omega}{\omega} = \frac{\sqrt{2}}{\omega\tau_{debunch}} \quad , \tag{23}$$

$$\frac{\Delta p}{p} = - \frac{1}{K\beta^2} \frac{\Delta\omega}{\omega} = 13.3 \, \frac{\Delta\omega}{\omega} \quad , \text{ where } K = \frac{1 - \alpha \; \gamma^2}{1 - \gamma^2} \tag{24}$$

The numerical coefficient in (24) is given for the parameters of NAP-M.

The results of measurements are shown in Fig. 5. In the cooling regime the momentum spread of the proton beam increased linearly with the proton current, so that

$$\frac{1}{I_p} \frac{\Delta p}{p} \simeq 0.5 \times 10^{-6} \; A^{-1} \quad .$$

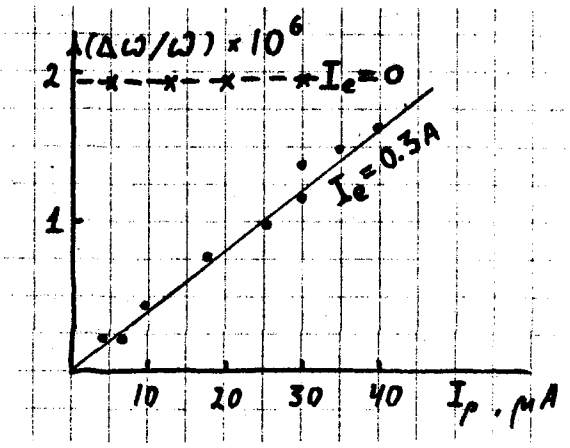

FIG. 5 - Measurements of proton revolution frequency spread by the debunching time method.

x x x x x x electron cooling is switched off
. . . . . electron cooling is switched on.

§ 8. THE EXPERIMENTS ON NEUTRALIZATION OF SPACE CHARGE IN THE ELECTRON BEAM

To neutralize the electron beam, two plates, located in the cooling region, were used. The plates were connected to have the same potential v_{pl} relative to the vacuum chamber wall. Neutralization was registered through measurement of the proton mean radial position as a function of the kinetic electron energy W_e ("drag" effect, see [I-6]). The results are presented in the Fig. 6. With a trapping potential $V_{pe} = -100$ V the displacement of the closed orbit in the straight section, where the measuring magnesium jet was located, agreed with the value calculated from the momentum compaction function of the storage ring NAP-M, without space charge. The small value of the trapping potential confirms that in our case electron space charge has only a small influence on the distribution of longitudinal electron velocities across the electron beam. In fact no significant influence of neutralization on the damping time was observed in our experiments.

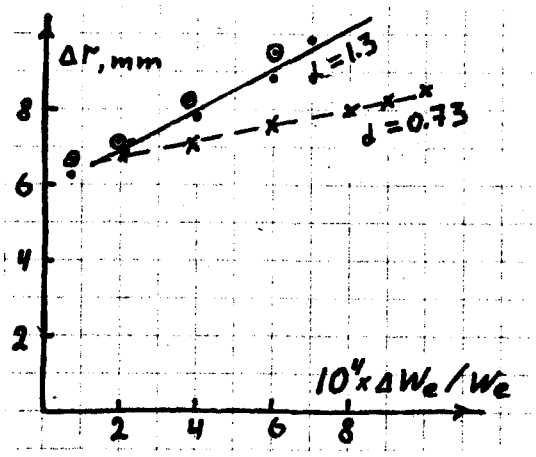

FIG. 6 - The neutralization of electron beam space charge.

Displacement of the radial beam position as a function of electron kinetic energy for different values of the potential on the clearing electrodes. Note change of the (deduced) value of the momentum compaction factor due to the electron space charge.

ooooooooo Upl = 0

. . . . . Upl = + 100 V

x x x x x Upl = - 100 V.

§ 9. THE ELECTRON COOLING OF BUNCHED PROTON BEAM [I-7]

In these experiments a decrase of the bunch length to an equilibrium dimension $\Delta l \simeq 5$ m was observed. (The NAP-M circumference is equal to 47 m, the first rf-harmonic is being used.) The measured damping time was 0.5 sec for $j_e = 0.3$ A/cm^2.

§ 10. THE "SUPERFAST" COOLING

It was recognized in our experiments, that during damping time measurements the amplitude of the betatron oscillation just after pulsing the deflector [I-6] is smaller, if electron cooling is on, then without electron cooling. This difference is connected with the resolution time (about 20 msec) of the magnesium jet device. The effect could be explained by the existence of "superfast" cooling - viz. betatron amplitude decrease by about 1 mm in less than 20 msec.

This effect, apparently, is connected with some kind of coherent damping of betatron oscillations [I-13]. We note that - for reasons which are not known so far - in some situations this effect was not observed. Further investigations are under way.

Figure 7a shows some results of measurements for different electron currents. Figure 7b is for fixed electron current but for different proton intensities.

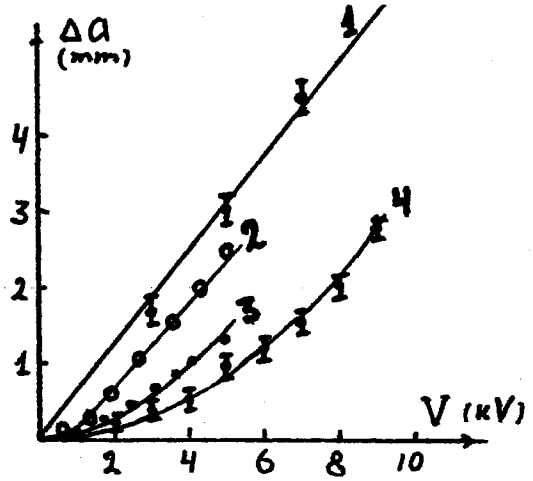

FIG. 7a - Difference in beam size before and after kick with electron cooling for different kick amplitudes V and different electron current values.

1. $I_e = 0$
2. $I_e = 100$ mA
3. $I_e = 200$ mA
4. $I_e = 400$ mA

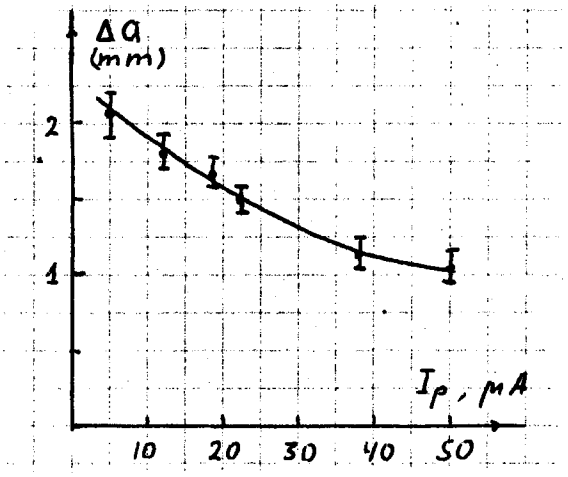

FIG. 7b - Difference in beam size before and after kick with electron cooling for different proton current values. $I_e = 400$ mA.

§ 11. THE ELECTRON COOLING OF LOW ENERGY PROTONS

It is interesting for some applications of electron cooling (see § 12 of this paper) to have the possibility to cool protons with very low energy. These experiments were made on NAP-M with protons at injection energy (1.4 MeV). It was possible to observe the qualitative effects of electron cooling: the increase of proton life time and the "drag effect" between the proton and electron beams during electron energy variations (Fig. 8). The damping time was not measured, because the experimental equipment for measurements at this low energy was not ready.

The results at 1.4 MeV are interesting also with respect to the electron cooling theory: at this low energy and for the cathode temperature ($T_{eff} \sim 0.1 \div 0.2$ eV) it is impossible to explain the existence of electron cooling effects if one assumes a uniform Maxwellian distribution of electron velocities.

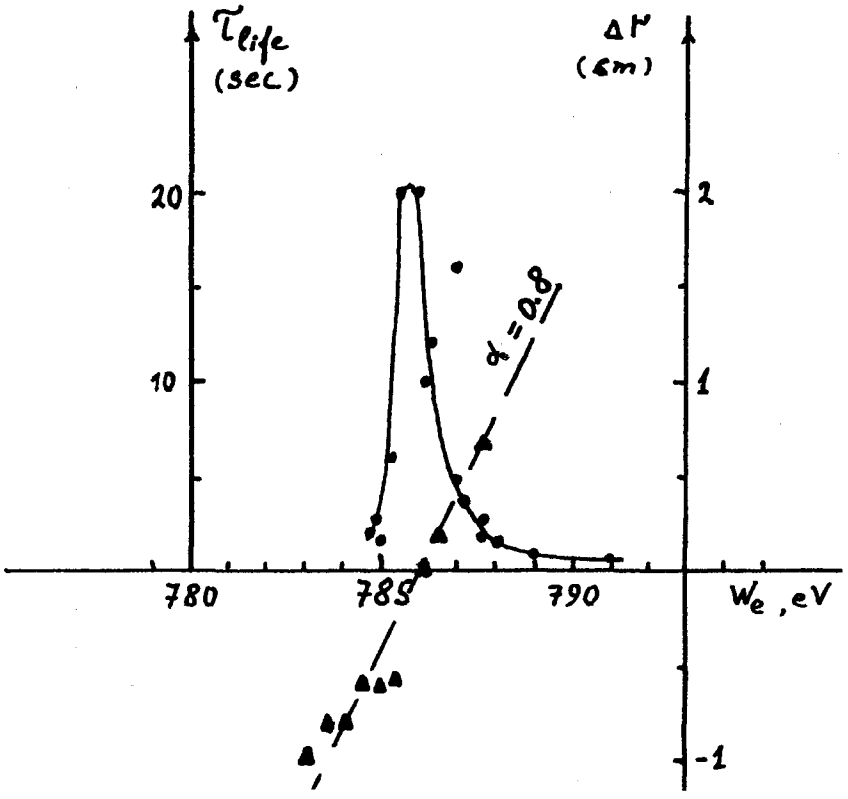

FIG. 8 - The results of electron cooling experiments for low energy protons.

..... the dependence of proton life-time on electron energy,

▲ ▲ ▲ the dependence of proton beam position from electron energy.

§ 12. THE POSSIBLE APPLICATIONS OF ELECTRON COOLING

We shall only list here possible applications, which are discussed in more details in reference [I-5,9].

1. $p\bar{p}$ - colliding beams with super-high energy and high luminosity

   2 x ∿ 300 GeV CERN, Batavia
   2 x 2 TeV Serpukhov / Novosibirsk

2. $p\bar{p}$ - Colliding beams in the intermediate energy region with high luminosity and very high energy resolution

   2 x 0.5 ÷ 20 GeV (Novosibirsk)
   study of structure resonances (e.g. ψ)→ $\Delta E < 10$ keV

3. The electron cooling of (heavy) ions and $\bar{p}$ for experiments using internal targets with very high energy resolution (spectrometry)

   $W_p \rightarrow 50$ MeV ÷ 20 GeV (?), $\Delta p/p < 10^{-5}$

4. The "protonium" study: $p\bar{p}$-bound state

   $\bar{p} + H^o \rightarrow (\bar{p}p) + e^-$

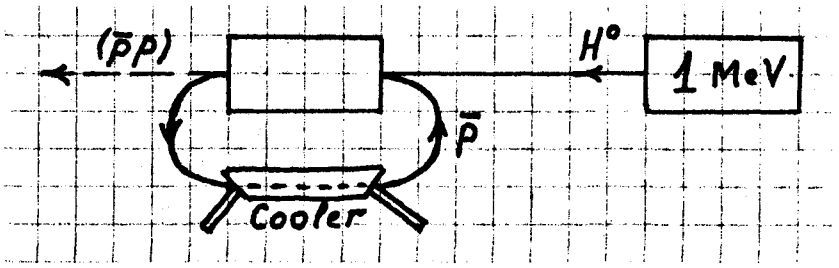

5. The "antihydrogen" production and study: $\bar{p} + e^+ \rightarrow \overline{H^o}$

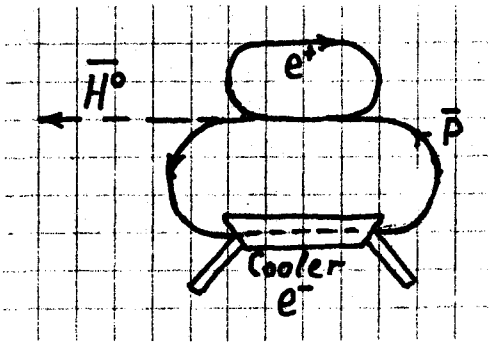

PART B

THE ELECTRON BEAM DEVICE FOR HEAVY PARTICLE COOLING EXPERIMENTS*

V.I. Kudelainen, I.N. Meshkov, R.A. Salimov

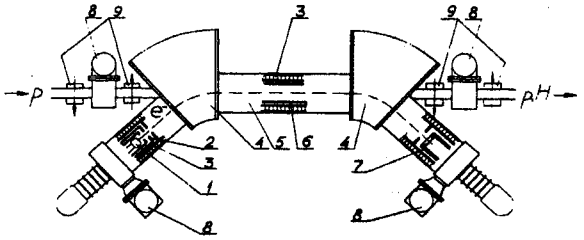

FIGURE 1 Layout of the electron-beam device: 1—electron gun; 2—anodes; 3—solenoids; 4—bending sections of electron beam; 5—cooling section; 6—vacuum chamber; 7—collector; 8—vacuum pumps; 9—correction magnets.

SUMMARY

The construction of the electron beam device and some experiments with the electron beam are described.

The following questions are discussed : the choice of electron beam parameters and the focusing system (it is shown that the only kind of focusing system suitable for cooling is one in which the electron beam is formed and transported in a homogeneous longitudinal magnetic field). Further subjects treated are the magnetic system, the electron gun with its special kind of optics, the electron collector, the mechanical tolerance and the influence of the magnetic field of the electron device on the particle trajectories in the heavy particle storage ring.

---

* Abbreviated translation of Preprint INP 72-70, Novosibirsk (1970), made in March 1977 at CERN by I.N. Meshkov. For this translation, the subject matter was updated, taking into account the progress made since 1970. The major part of the preprint is also contained in Ref. II-4.

CONTENTS

THE LIST OF SYMBOLS

$A = \sqrt{\frac{eI}{\beta^3\gamma^3 mc^3}}$	the space charge parameter
a	the radius of the electron beam cross section (round beam)
2a,2b	the radial and vertical dimensions of an electron beam of elliptical cross section
c	the velocity of light
D	the spacing between turns in the correction coils (§ 4)
d	- the pitch of the solenoid coil (§ 4) - the distance between gun anodes (§ 5) - the length of the longitudinal magnetic field region in the storage ring
e	the electron charge
E	the electric field strength
f	- the focal length (§ 2, 3) - the perturbation force
H, H_o	the magnetic field strength
H_x,H_y	the magnetic field components (§ 3)
$H_\perp$, $H_{\perp\perp}$	the transverse components of the magnetic field (§ 3,4)
H_ρ	the magnetic bending field (§ 3)
j,I	the current density and the total current of the electron beam
ΔI	the electron beam losses
m,M	the electron, ion mass
p, p_m	the electron, ion momentum
P	the residual gas pressure
P_a,P_r	the active, reactive power

Q_a, Q_b, Q_o	the focusing functions (§ 1)
r, θ , z	the cylindrical co-ordinate system, in which the z-axis is directed along the beam axis (magnetic field direction)
r, z, s	a co-ordinate system used in calculations of the storage ring; the z-axis is parallel to the direction of the bending magnetic field (§ 9)
R_s	the average radius of the storage ring
R_o	the radius of curvature of the magnetic field line (§ 3, 4)
R_c, r_c	the cross-section radius of the solenoids (§ 4)
s	the longitudinal co-ordinate along the ideal orbit
V, V_{tot}	the acceleration voltage on the gun
v, $v_{/\!/}$, $v_{\perp}$	the particle velocity and its components
W	the kinetic energy
x, y, z	the curved frame used for the bending region; the z-direction is parallel to the electron velocity, the y-axis is parallel to the bending axis (§ 3)
$\beta = v/c$, $\gamma = (1-\beta^2)^{-\frac{1}{2}}$	relativitstic factors
η	the ratio of cooling region length to the storage ring circumference
θ	the azimuthal co-ordinate
θ_e	the ratio of transverse velocity (of electrons, protons) to the longitudinal velocity
$\theta_{\perp}$	the same for transverse velocities spread
θ_o	the angle between the axes of the electron and the proton beams

$\lambda = 2\pi pc/eH$ the Larmor revolution length

τ_e the cooling time

$\omega = \frac{eH}{pc}$, $\omega_M = \frac{eH}{p_M c}$ } the cyclotron frequency of electron, ion

ϕ_o the bending angle

§ 1. - The electron beam for heavy particle cooling

1.1 The choice of focusing system

At low energy the cooling time is proportional to the third power of the electron transverse velocity [I.1,2]. It is necessary to avoid the systematic transverse velocity $\theta_o v_{//}$ which appears, if the axes of the electron and the proton beam are not parallel, and the spread of transverse electron velocities $\theta_T = (v_\perp)_T / v_{//}$, which determines the "temperature" of the electron beam.

The value of θ_T depends on the kind of focusing system (optics). It is useful to calculate as completely as possible the focusing properties of the optics system to determine the minimum possible value of θ_T.

Let us first assume that the electron beam, which is formed with some kind of accelerating system (electron gun, for example) enters a transport channel, such that its parameters are matched to the input parameters of the channel. We shall neglect the phase space volume of the electron beam. The envelope equations can be written in this case as [IV-1]

$$\frac{d^2a(z)}{dz^2} + Q_a(z) \cdot a(z) - \frac{4A^2}{a+b} = 0$$

$$\frac{d^2b(z)}{dz^2} + Q_b(z) \cdot b(z) - \frac{4A^2}{a+b} = 0 \qquad (1.1)$$

Here, $A^2 = eI/\beta^3\gamma^3 mc^3$.

I is the electron beam current; a(z), b(z) the transverse dimensions of the beam which are determined by the character of the focusing system; $Q_a(z)$, $Q_b(z)$ the functions which describe the focusing properties of the transport system.

The minimum transverse velocities will be obtained, if the beam envelopes a(z) and b(z) are constant, but this is possible only if the focusing is constant and the focusing force compensates the defocusing space charge force of the electron beam in each point of the trajectory :

$$Q_a = \frac{4A^2}{a(a+b)} = \text{const.} \qquad (1.2)$$

This situation can be realized in a "weak" focusing accelerator (or in a bending magnet). But it is impossible to achieve a straight transport system with constant focusing in both planes.

If we have an alternating gradient focusing system, we can satisfy equation (1.2) only for the average forces. The beam envelope oscillates in this case, and only the transverse beam dimension, averaged over these oscillations, can be made constant. If the oscillations are small, it is convenient to use the linear approximation for the solution of equations (1.1) :

$$\begin{aligned} a(z) &= a(z)\left[1+\xi_a(z)\right] \\ b(z) &= b(z)\left[1+\xi_b(z)\right] \\ \xi(z) &\ll 1 \end{aligned} \qquad (1.3)$$

After substitution of (1.3) in (1.1) and after elimination of the rapidly oscillating terms, the equation for the slow changing functions has the form :

$$\begin{aligned} a'' + (\overline{Q_a\xi_a} + \overline{Q_a})a - \frac{4A^2}{a+b} &= 0 \,, \\ b'' + (\overline{Q_b\xi_b} + \overline{Q_b})b - \frac{4A^2}{a+b} &= 0 \end{aligned} \qquad (1.4)$$

The equation for oscillating terms (up to the first order) also follows from (1.1) :

$$\begin{aligned} \xi_a'' + \frac{4A^2}{a(a+b)}\,(\xi_a + \xi_b) + Q_a(z)\,(1+\xi_a) &= 0 \\ \xi_b'' + \frac{4A^2}{b(a+b)}\,(\xi_a + \xi_b) + Q_b(z)\,(1+\xi_b) &= 0 \end{aligned} \qquad (1.5)$$

The simplest variant of our alternating gradient focusing system is characterized by :

$$Q_a(z) = Q_o \sin \Omega Z = \pm\, Q_b(z) \qquad (1.6)$$

The sign (+) in (1.6) has to be used, if a focusing system with axial lenses is used, the sign (-) for quadrupole lenses.

For a small length of the focusing period, when

$$\Omega >> \sqrt{Q_o} \ , \ \frac{A}{a_o} \tag{1.7}$$

the average beam dimension will be constant, if

$$a = b = \frac{2\Omega A}{Q_o} \tag{1.8}$$

(the case a=b is used for simplicity only). The envelope oscillations can be written as :

$$\xi_a(z) = \frac{Q_o}{\Omega^2} \sin \Omega z = \pm \xi_b(z) \tag{1.9}$$

The substitution of (1.8,9) in the expression for θ_T

$$\theta_T = \left[\left(\frac{dx_a}{dz} \right)^2 + \left(\frac{dx_b}{dz} \right)^2 \right]^{\frac{1}{2}} \tag{1.10}$$

gives

$$(\theta_T)_{min} = 2\sqrt{2}\, A = \left(\frac{8eI}{\beta^3 \gamma^3 m c^3} \right)^{\frac{1}{2}} \tag{1.11}$$

It is noted from (1.11) that the value of $(\theta_T)_{min}$ is determined by the total beam current and does not depend on the details of focusing system.

If the beam transport in a longitudinal magnetic field is used, and the electron source is located outside the magnetic field, the minimum transverse velocity corresponds to the well known condition of Brillouin flow. In this case the equilibrium dimension of the electron beam is described by expression (1.2) if one takes

$$Q_o = \frac{\omega^2}{4} \tag{1.12}$$

The radial velocity of the electrons is zero in the case of Brillouin flow, and the total transverse velocity is equal to the azimuthal rotation velocity, so that :

$$(\theta_T)_{min} = \sqrt{2}\,A = \left(\frac{2eI}{\beta^3\gamma^3 mc^3}\right)^{\frac{1}{2}} \tag{1.13}$$

This is analogue to (1.11).

A more favourable result can be obtained if the electron source is located inside the longitudinal magnetic field. It will be shown in the next paragraph that in this case , if the magnetic field is homonegeous enough, and field strength is unlimited, the space charge effect can be made as small as

$$(\theta_T)_{min} = \frac{4A^2}{\omega a} = \frac{4I}{\beta^2\gamma^2 c\,Ha} \tag{1.14}$$

1.2 The space charge effects

The space charge of the electron beam produces also the spread of the longitudinal electron velocities. If the electron beam does not trap ions, the potential inside the beam is proportional to the distance from the beam axis :

$$\Delta U(r) = \frac{I}{\beta c} \cdot \frac{r^2}{a^2} = \frac{30\,I(Amp)}{\beta} \cdot \frac{r^2}{a^2} \tag{1.15}$$

In order to meet the conditions for the stability of the electron cooling process (connected with the drag from the electron beam on the proton beam - see Ref. I-2 & I-6, Part VII) one has to make sure that the gradient of longitudinal electron velocities remains small enough

$$\frac{d(v_e)_{//}}{dr} < \frac{(dv_p)_{//}}{dr} \equiv \alpha \frac{\beta c}{\gamma^2 R_s} \tag{1.16}$$

where α is the average momentum compaction parameter of the heavy particle storage ring, R_s, its average radius.

From expressions (1.15, 1.16), the electron current limit follows as :

$$I \lesssim \alpha \frac{mc^3}{e} \beta^3\gamma \frac{a}{2R_s} \tag{1.17}$$

This is a very strong limitation, and it signifies that the electron current is very small in comparison with the virtual cathode limitation :

$$I << \frac{mc^3}{e} \cdot \frac{(\gamma^{2/3} - 1)^{3/2}}{1 + 2\ell n \frac{\rho}{a}} \qquad (1.18)$$

where a and ρ are the radii of the beam and the vacuum chamber cross sections. The condition (1.18) is written down here only for comparison.

It is possible to try "to fraud" the condition (1.17), for example by compensating the electron beam space charge with ions of the residual gas. But, in this case, the plasma beam instabilities are able to develop, if the beam current is large enough. The most dangerous instabilities have the threshold current [IV-2] :

$$I_{thres} \simeq \frac{mc^3}{e} \cdot \frac{\beta^3\gamma^3}{1 + 2\ell n \frac{\rho}{a}} \cdot \frac{1}{1 + \frac{L_{beam}}{a}} \cdot \frac{pc}{eHa} \qquad (1.19)$$

where L_{beam} is the beam length, p the electron momentum. The threshold is approximately 1 A for the parameters : L_{beam} = 1 m, β = 0.35 ($W_e \simeq$ 35 keV), $\rho \simeq 3\ a$ = 1,5 cm, H = 1 kG.

---

* A comment during translation

The conditions (1.16, 1.17) can be derived from the conditions of stability of the drag process during the heavy particle cooling process (for details, see Ref. I-6, Part VII).

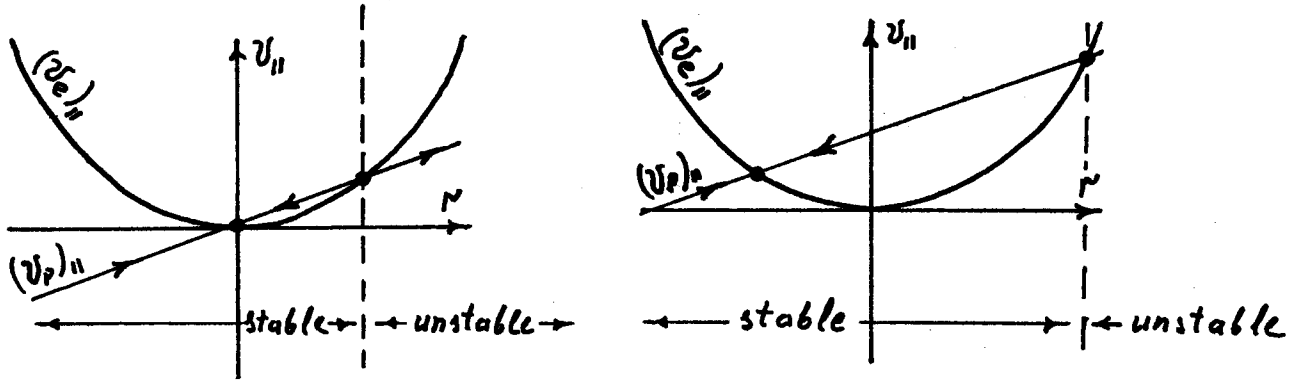

To "accept" the whole proton beam, it is possible to move the working point. (Right hand figure)

But the tolerable difference between electron velocities on the beam axis and near its boundary is not very large; in the extreme case, it is necessary to satisfy the condition

$$\frac{\Delta v//}{v} < \theta_T$$

or

$$I \lesssim \frac{mc^3}{e} \beta^3\gamma^2 \theta_T \qquad (1.20)$$

This condition permits for NAP-M parameters : $I \sim 1$ A.

The error on the average electron velocity leads to a "monochromatic instability" [I-2]. This leads to the conditions for the stability of the electron energy and the tolerable difference in the average energies of electrons and protons and also imposes limits on the angle θ_o between the axes of the electron and the proton beams as follows :

$$\frac{\Delta W}{W} \lesssim (\gamma + 1) \theta_T \qquad (1.21)$$

$$\theta_o < \theta_T \qquad (1.22)$$

---

* A comment during translation

The tolerance on electron energy fluctuations must be very much more severe to use the advantage of a "flattened" distribution (Ref. I-6, I-7). It is necessary in fact, in this case, to ensure the condition :

$$\Delta W_\sim < T_{cathode} \sim 0.1 \text{ eV} \qquad (1.23)$$

instead of condition (1.21).

§ 2. - The electron beam in the longitudinal magnetic field

2.1 The general case

The influence of different kinds of perturbations on the electron motion will be considered in this paragraph.

It is useful in this case to work in a cylindrical frame (r,θ,z), where the z-axis is directed along the beam axis. The equations of motion are :

$$\frac{1}{\beta\gamma} \cdot \frac{d}{dz} (\beta\gamma \frac{dr}{dz}) + \frac{\omega^2}{4} (1 - \frac{M^2}{H_z^2 r^4}) r = \frac{eE_r}{\beta^2\gamma mc^3} - \frac{eH_\theta}{\beta\gamma mc^2} \qquad (2.1)$$

$$\gamma m\dot{\theta} r^2 + \frac{eH_z r^2}{2c} = e \int_o^t r\, E_\theta\, dt + \frac{eM}{2c} \qquad (2.2)$$

Here E, H are the components of the electric and magnetic fields, ω is the cyclotron frequency, M is the integral of motion

$$\omega = \frac{eH}{pc} \quad , \quad M = H_o r_o^2 \qquad (2.3)$$

The index "o" corresponds to the initial conditions.

Let us consider the case of a cathode which is located in the longitudinal magnetic field. We shall find the solution for small transverse velocities and displacements, so that

$$r \backsim r_o(1 + \xi(z)) \quad ; \quad \xi(z) \ll 1 \qquad (2.4)$$

Let us assume also $E_\theta = 0$ and let E_r and H_θ be the self fields of the electron beam. In this case, we have :

$$\dot{\theta}(z) = - \frac{eH}{\gamma mc} (\xi + \frac{\Delta H}{H}) \qquad (2.5)$$

$$\frac{d^2\xi}{dz^2} + \omega^2 \xi = \frac{2A^2}{a^2} - \omega^2 \frac{\Delta H}{2H} \qquad (2.6)$$

where $$A^2 = \left(\frac{eI}{\beta^3\gamma^3 mc^3}\right)^{\frac{1}{2}} , \qquad (2.7)$$

a is the electron beam radius, H(z) the difference between the longitudinal magnetic field strength at points z = 0 and z.

The solution of the equations (2.5, 2.6) is :

$$\xi(z) = \frac{1}{\omega r_o}\left(\frac{dr}{dz}\right)_o \sin \omega z + \frac{2A^2}{\omega^2 a^2}(1 - \cos \omega z) - \frac{\omega}{2}\int_{z_o}^{z} \frac{\Delta H(x)}{H} \; x$$

$$x \sin \omega(z-x)\, dx \qquad (2.8)$$

It follows from expressions (2.5) and (2.8) that in an ideal homogeneous longitudinal magnetic field and without space charge of the electron beam, the projection of the particle trajectories on the (r,θ) plane are Larmor circles with a radius $\rho_L = p_\perp c/eH$ and the centre located at

$$r_L = r_o - \rho_L$$

If the perturbations of the magnetic field are axial-symmetrical, and the symmetry axis coincides with the beam axis, the field perturbations and the beam space charge produce a beam rotation around this axis with the frequency :

$$\frac{\dot{\theta}}{v_{//}} = \omega\left(\bar{\xi} + \frac{\Delta H}{2H}\right) = \frac{2A^2}{\omega a^2} + \omega\,\frac{\Delta H}{2H} = \frac{2\ I}{\beta^2\gamma^2 cHa} + \frac{e\Delta H}{2pc} \qquad (2.9)$$

and secondly the expansion of the Larmor radius, that corresponds to an increase of the transverse velocity of the particle. The total transverse velocity

$$v_\perp = v_{//}\sqrt{\left(\frac{r\dot{\theta}}{v}\right)^2 + \left(\frac{dr}{dz}\right)^2} \qquad (2.10)$$

can be calculated, if we use the expressions (2.5) and (2.8). The result of general calculations is too bulky and it is more convenient to use simpler expressions, which describe the influence of each kind of perturbation separately. If the perturbations are small, the results are additive. It is easy to obtain in this way from (2.5), (2.8) and (2.10) expressions for the influence of space charge

$$\frac{v_\perp}{v_{//}} \lesssim \frac{4A^2}{\omega a} \sin\frac{\omega z}{2} \lesssim \frac{4\ I}{\beta^2\gamma^2 cHa} \qquad (2.11)$$

The inhomogeneities of the longitudinal magnetic field produce a transverse velocity

$$\frac{v_\perp}{v_{/\!/}} \lesssim \frac{\omega a}{2} \sqrt{\left[\omega \int_{z_o}^{z^*} \frac{\Delta H(x)}{H} \cos \omega(z-x)\, dx\right]^2 + \left[\frac{\Delta H(z^*)}{H} - \omega \int_{z_o}^{z^*} \frac{\Delta H(x)}{H} x \sin \omega(z-x)\, dx\right]^2} \qquad (2.12)$$

A change of arguments in the integrals in (2.12) gives

$$\frac{v_\perp}{v_{/\!/}} \lesssim \frac{\omega a}{2} \sqrt{\left[\omega \int_{o}^{\Delta} \frac{\Delta H(\chi)}{H} \cos \omega\chi\, d\chi\right]^2 + \left[\frac{\Delta H(z^*)}{H} - \omega \int_{o}^{\Delta} \frac{\Delta H(\chi)}{H} \sin \omega\chi\, d\chi\right]^2} \qquad (2.13)$$

where $\chi = z-x$ and z_o, z^* are the co-ordinates of the beginning and the end of the field perturbation region.

The integration in (2.13) has to proceed along the direction of decreasing z so that

$$\Delta H = \begin{cases} 0, \text{ when } z = z_o \text{ and } \chi = \Delta \\ \Delta H(z^*), \text{ when } z = z^* \text{ and } \chi = 0 \end{cases}$$

This is negligible, if the field perturbation is local (i.e. $H(z^*) = 0$) and $H(z)$ is a symmetrical function of argument z (with respect to the centre of perturbation region (Fig. 2). However it is substantial if the field strength increases (or decreases) (Fig. 3). In both cases, the final result depends on the character of the function $\Delta H(z)$. Estimates for some important cases are given later. The characteristic parameter of the field variation length is the **Larmor** wavelength.

$$\lambda = 2\pi pc/eH \qquad (2.14)$$

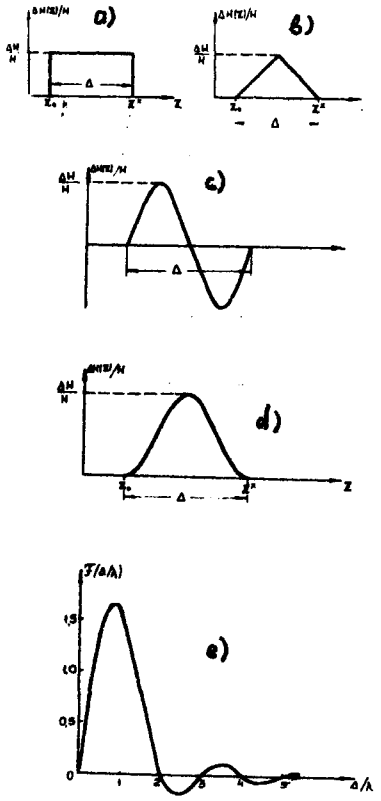

Fig. 2. Explanation in the text.

2.2 The field perturbations

The local perturbation

1) The fast field variation (Fig. 2a)

$$v_\perp / v_{//} \lesssim 2\pi \frac{a}{\lambda} \cdot \frac{\Delta H}{H} \sin \pi \frac{\Delta}{\lambda} \tag{2.15}$$

If $\Delta << \lambda$, (the short fast perturbation) (2.25) gives

$$v_\perp / v_{//} \lesssim 2\pi^2 \frac{a\Delta}{\lambda^2} \cdot \frac{\Delta H}{H} \tag{2.16}$$

2) The "triangular perturbation (Fig. 2b) :

$$v_\perp / v_{//} \lesssim 4 \frac{a}{\Delta} \cdot \frac{\Delta H}{H} \sin^2 \pi \frac{\Delta}{2\lambda} \tag{2.17}$$

3) The "sinewave" perturbation (Fig. 2c) :

$$v_\perp / v_{//} \lesssim \frac{2\pi a\Delta}{\lambda^2} \cdot \frac{\Delta H}{H} \cdot \frac{\sin \pi \frac{\Delta}{\lambda}}{1 - \frac{\Delta^2}{\lambda^2}} \tag{2.18}$$

It follows from (2.17) :

$$v_\perp/v_{/\!/} \lesssim \begin{cases} \text{a)} \quad 2\pi^2 \frac{a\Delta^2}{\lambda^2} \cdot \frac{\Delta H}{H} & , \quad \Delta << \lambda \\ \text{b)} \quad \pi^2 \frac{e\Delta}{\lambda^2} \cdot \frac{\Delta H}{H} & , \quad \Delta = \lambda \\ \text{c)} \quad 0 & , \quad \Delta = (k+1)\lambda, \; k = 1,2,3... \\ \text{d)} \quad 2\pi \frac{a}{\Delta} & , \quad \Delta >> \lambda \end{cases} \tag{2.19}$$

4) The "cosine half-wave" slow variation (Fig. 2d)

The field variation is approximated in this case by the function :

$$\Delta H(z) = \frac{\Delta H}{2} (1 - \cos 2\pi \frac{z}{\Delta}) \tag{2.20}$$

This approximation has a rather general character and will therefore be discussed in detail. The result

$$v_\perp/v_{/\!/} \lesssim \pi \frac{a}{\lambda} \cdot \frac{\Delta H}{H} \cdot \frac{\sin \pi \frac{\Delta}{\lambda}}{1 - (\frac{\Delta}{\lambda})^2} \tag{2.21}$$

is illustrated in Fig. 2e, where the form factor function

$$F(x) = \frac{\sin \pi x}{1 - x^2} \tag{2.22}$$

is given. This form factor function decreases very fast, when $x = \frac{\Delta}{\lambda} > 2$ and x continues to increase. This situation corresponds to the adiabatic field variation.

$$v_\perp/v_{/\!/} \lesssim \begin{cases} \text{a)} \quad \pi^2 \frac{a\Delta}{\lambda^2} \cdot \frac{\Delta H}{H} & , \quad \Delta << \lambda \\ \text{b)} \quad \frac{a}{\lambda} \cdot \frac{\Delta H}{H} & , \quad \Delta \quad 0.8375\,\lambda \text{ (maximum F(x))}, \\ \text{c)} \quad 0 & , \quad \Delta = (k+1)\lambda \, , \; k = 1,2,3... \\ \text{d)} \quad \pi \frac{a\lambda}{\Delta^2} \cdot \frac{\Delta H}{H} & , \quad \Delta >> \lambda \end{cases} \tag{2.23}$$

The addition of a constant field to the original field level

Let us consider the case when the field receives a constant addition ΔH over a distance Δ, i.e. for $z > z^*$ the field is homogeneous too, with the field strength $H(z > z^*) = H + \Delta H$. As before there are some interesting cases of field variation :

1) The fast field variation (Fig. 3a)

$$v_\perp / v_{//} \lesssim \pi \frac{a}{\lambda} \cdot \frac{\Delta H}{H} \tag{2.24}$$

(Compare this to (2.15, 2.16)).

2) The linear variation (Fig. 3b)

$$\Delta H(z) = H \frac{z}{\Delta} , \quad 0 < z < \Delta$$

In this case,

$$v_\perp / v_{//} \lesssim \frac{a}{\Delta} \cdot \frac{\Delta H}{H} \sin \pi \frac{\Delta}{\lambda} \tag{2.25}$$

If $\Delta << \lambda$, the both results (2.24, 2.25) coincide.

3) The slow variation (Fig. 3c)

$$\Delta H(z) = \frac{\Delta H}{2} (1 - \cos \pi \frac{z}{\Delta}) , \quad 0 \leq z \leq \Delta \tag{2.26}$$

The transverse velocity variations can be written in this case as

$$v_\perp / v_{//} \leq \frac{\pi a}{\lambda} \cdot \frac{\cos \pi \frac{\Delta}{\lambda}}{(\frac{2\Delta}{\lambda})^2 - 1} \cdot \frac{\Delta H}{H} \tag{2.27}$$

Special cases of (2.27) are :

$$v_\perp / v_{//} \lesssim \begin{cases} a) \quad \pi \frac{a}{\lambda} \cdot \frac{\Delta H}{H} , & \Delta << \lambda \\ b) \quad \frac{\pi^2}{4} \cdot \frac{a}{\lambda} \cdot \frac{\Delta H}{H} , & \Delta = \frac{\lambda}{2} \\ c) \quad 0 , & \Delta = (k+\frac{1}{2})\lambda, \; k = 1,2,3... \\ d) \quad \frac{\pi}{4} \cdot \frac{a\lambda}{\Delta^2} \cdot \frac{\Delta H}{H} , & \Delta >> \lambda \end{cases} \tag{2.28}$$

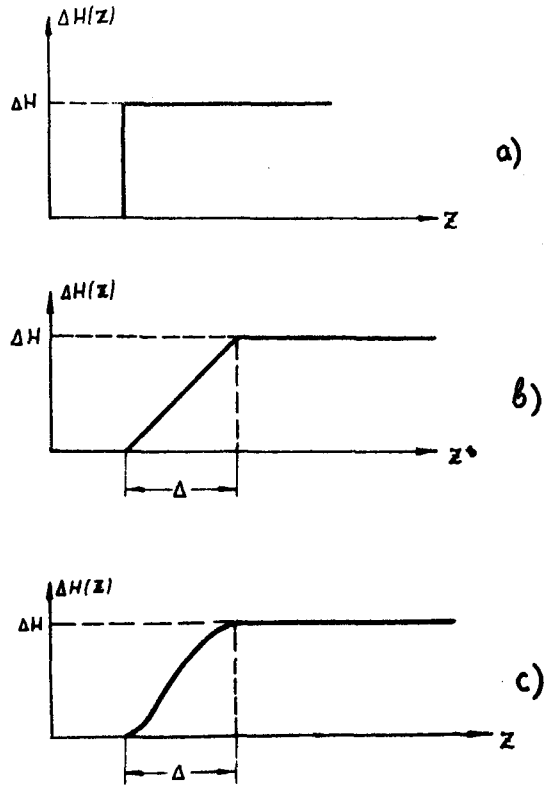

Fig. 3. Explanation in the text.

The most important results of the description of the perturbation influence are expression (2.19d) and (2.28d) which explain our method of the "steering" of the electron beam : it is possible to change the position and the dimensions of electron beam without introduction of significant perturbations into the beam, if the field variations are slow enough in comparison with λ .

---

* A comment during translation

The last theoretical results show that to use "fast" cooling (the magnetized electron beam with flattened distribution - see Part I) it is necessary to have a constant longitudinal magnetic field in the cooling region.

§ 3. - The bending of the electron beam into the cooling section

To guide the electron beam in the cooling region (the region of interaction between electrons and protons) it is necessary to bend the entire electron beam by the same angle (this angle being defined by the geometry of the device). It is important (at the same time!) not to distort the longitudinal magnetic field, as was shown in § 2. The question of a solenoid design will be discussed in § 4. Let us assume that the bending region is like a part of a toroidal solenoid and that it has field lines with varying curvature along the bending azimuth. The electron beam perturbation in the bending region will be small, if the particle trajectories coincide with a good accuracy with the field lines of the toroidal longitudinal magnetic field. To achieve this, it is necessary to add in this region a magnetic bending field, which is parallel to the axis of the bend.

3.1 The particle trajectories in the bending region

Let us use a frame which moves along the trajectory of the central particle inside the beam : the co-ordinate z is being measured along this central trajectory, the co-ordinates x and y correspond to radial and axial displacements. And let us assume that the central tractory is curved, with a curvature radius $R_o(z)$. As before, let us use the paraxial equations. In this case [IV-4] :

$$\begin{aligned} &\ddot{x} - \left(1 - \frac{x}{R_o}\right) \frac{v^2}{R_o} = - \frac{ev}{\gamma mc} \left(H_y + H_\rho\right) + \frac{\dot{e}y}{\gamma mc} H_z \,, \\ &\ddot{y} = - \frac{\dot{e}x}{\gamma mc} H_z + \frac{ev}{\gamma mc} H_x \end{aligned} \qquad (3.1)$$

The longitudinal velocity v is assumed constant.

In the paraxial approximation the coupling between the components of the longitudinal magnetic field is negligible and, assuming that the field perturbations are axially-symmetrical, we may write :

$$H_x = H_x^o(z) - \frac{x}{2} \cdot \left(\frac{dH_z^o(z)}{dz}\right) ,$$

$$H_y = H_y^o(z) - \frac{y}{2} \cdot \frac{dH_z^o}{dz} \quad , \qquad (3.2)$$

$$H_z(z,x) = H_z^o \cdot (1 - \frac{x}{R_o})$$

Index "o" here refers to the value on the central trajectory. The last equation in (3.2) reflects the particularity of the toroidal solenoid. We shall from now onwards drop (for conciseness) the superscript "o" for the H_z^o components. It follows from (3.1) and (3.2) that

$$\begin{aligned} &\frac{d^2x}{dz^2} + \frac{x}{R_o^2} - \omega \frac{dy}{dz} - \frac{y}{2} \cdot \frac{d\omega}{dz} = - \omega \frac{H_y^o}{H_z} + \frac{1}{R_o} - \frac{eH_\rho}{pc} \quad , \\ &\frac{d^2y}{dz^2} + \omega \frac{dx}{dz} + \frac{x}{2} \cdot \frac{d\omega}{dz} = \omega \frac{H_x^o}{H_z} \end{aligned} \qquad (3.3)$$

If the magnetic field is homogeneous along the longitudinal direction ($d\omega/dz = 0$) and the bending field is correct ($eH_\rho(z)R_o(z) = pc$), the flat field line with a curvature radius $R_o(z)$ is the trajectory of the central particle.

3.2 The free oscillations

The homogeneous equations (3.3) describe the free oscillations of particles near the central trajectory, when

$$d\omega/dz = 0 \quad ; \quad R_o(z) = \text{const.}$$

The oscillation frequencies are the solution of the characteristic equation

$$\begin{vmatrix} \kappa^2 + \frac{1}{R_o^2} & -\omega\kappa \\ \omega\kappa & \kappa^2 \end{vmatrix} = 0 \qquad (3.4)$$

It leads to

$$\kappa_{1,2} = \pm i\omega \sqrt{1 + \frac{1}{(\omega R_o)^2}} \equiv i\Omega$$

$$\kappa_{3,4} = 0$$

The solution for the particle trajectory is :

$$
\begin{aligned}
x(z) &= \overset{(i)}{x_o} - \overset{(ii)}{x_o \frac{1-\cos \Omega z}{1+\omega^2 R_o^2}} + \overset{(iii)}{\frac{1}{\Omega}\left(\frac{dx}{dz}\right)_o \sin \Omega z} + \overset{(iv)}{\frac{1}{\omega}\cdot\left(\frac{dy}{dz}\right)_o \frac{1-\cos \Omega z}{1+\omega^2 R_o^2}}, \\
y(z) &= \overset{(v)}{y_o} + \overset{(vi)}{\left[x_o + \frac{1}{\omega}\left(\frac{dx}{dz}\right)_o\right]\frac{\omega z}{1+\omega^2 R_o^2}} - x_o - \overset{(vii)}{\cdot\left(\frac{\sin \Omega z}{1+\omega^2 R_o^2}\right)} \\
&\quad + \overset{(viii)}{\frac{\omega}{\Omega^2}\left(\frac{dx}{dz}\right)_o (1-\cos \Omega z)} + \frac{1}{\omega}\left(\frac{dy}{dz}\right)_o \overset{(ix)}{\left(\frac{\omega^2 R_o^2}{1+\omega^2 R_o^2}\right)} \sin \Omega z
\end{aligned}
\tag{3.6}
$$

Index "o" here refers to the initial values of the parameters (at the entry to the bending region).

Each member of the cumbersome expressions (3.6) has a very simple physical meaning. Members (i), (iii), (v) and (ix) are determined by the initial conditions; (iv), (vii) and (viii) describe the coupling oscillations of the particle in the (x,y) plane, (vi) the beam expansion in the y-direction due to the drift caused by the centrifugal force and the field; and (ii) the well-known aperture effect of the bending magnets (a particle moving outside the central trajectory has on the exit of the bending magnet a transverse velocity, which is proportional to x_o). The last effect is decreased by the longitudinal magnetic field and for $\omega R_o >> 1$, one has

$$
\frac{v_\perp}{v_{//}} \simeq \frac{x_o \lambda}{\pi R_o^2} \sin \frac{\pi \Delta z}{\lambda} \qquad , \qquad \omega R_o >> 1 \tag{3.7}
$$

where

$$
\Delta z = \int_o^{\phi_o} R_o(\phi)\, d\phi
$$

is the length of the bending region measured along the central trajectory.

There is a very important circumstance : the results (3.6, 3.7) are true only for the case of an electron source, which is located inside the longitudinal magnetic field. In the situation, where the source is located outside the field, it is necessary to take into account in equations (3.1, 3.3), the members with ω'.

3.3 The solution for "external" forces

The influence of different perturbations on the particle motion in the bending region will now be valid for strong longitudinal magnetic field, in an approximation described by :

$$\omega R_o >> 1$$

In this case the equations (3.3) can be written as :

$$\begin{aligned} x'' - \omega y' &= f_1(z) \\ y'' - \omega x' &= f_2(z) \end{aligned} \tag{3.8}$$

The particular solution of these equations is :

$$\begin{aligned} x(z) &= \frac{1}{\omega} \int_{z_o}^{z} f_1(\chi) \sin \omega(z-\chi) d\chi - \frac{1}{\omega} \int_{z_o}^{z} f_2(\chi) \cos \omega(z-\chi) d\chi \\ &\quad + \frac{1}{\omega} \int_{z_o}^{z} f_2(\chi)\, d\chi \\ y(z) &= \frac{1}{\omega} \int_{z_o}^{z} f_1(\chi) \cos \omega(z-\chi) d\chi + \frac{1}{\omega} \int_{z_o}^{z} f_2(\chi) \sin \omega(z-\chi) d\chi \\ &\quad - \frac{1}{\omega} \int_{z_o}^{z} f_1(\chi) d\chi \end{aligned} \tag{3.9}$$

The transverse velocity perturbations which are connected with "external forces" $f_{1,2}(z)$ are described by

$$\begin{aligned} \left(\frac{v_\perp}{v_{/\!/}}\right)^2 &= \left[\int_o^{\Delta} f_1(\chi) \cos \omega\chi \, d\chi + \int_o^{\Delta} f_2(\chi) \sin \omega\chi \, d\chi\right]^2 \\ &\quad + \left[\int_o^{\Delta} f_1(\chi) \sin \omega\chi \, d\chi - \int_o^{\Delta} f_2(\chi) \cos \omega\chi \, d\chi\right]^2 \end{aligned} \tag{3.10}$$

The same notation is used, as in (2.13), and the remarks about the integration also apply to the present case.

Let us consider now separately the influence of each kind of external perturbation..

The inhomogeneity of the longitudinal magnetic field is described by the terms with $\omega' x/2$ and $\omega' y/2$ in the equations (3.3). After the substitution :

$$f_1(z) = \frac{\omega' y_o}{2} \quad , \quad f_2(z) = \frac{\omega' x_o}{2}$$

and integration of (3.10) by parts, it is easy to obtain (2.13) if we note that

$$\Delta H(\chi) = \begin{cases} \Delta H\ (z^*) & \chi = 0 \\ 0 & \chi = \Delta \end{cases}$$

$$x_o^2 + y^2 = a^2$$

This means that the results of § 2 can be used to estimate the influence of axially symmetrical perturbations of the longitudinal magnetic field.

The bending field errors produce the external force

$$\rho(z) = \frac{1}{R_o(z)} - \frac{eH_\rho(z)}{pc} \tag{3.11}$$

By virtue of (3.10) :

$$\frac{v_\perp}{v_{//}} \lesssim \frac{\lambda \rho_{max}}{\pi} = \frac{\lambda}{\pi R_o} \cdot \frac{\Delta H}{H_\rho} \tag{3.12}$$

The inequality (3.12) can be used to make a crude estimate of the order of magnitude and for more exact estimations it is necessary to use formulae (2.15, 2.23) replacing :

$$\frac{\Delta H}{H} \longrightarrow \frac{\rho_{max} \lambda^2}{2\pi^2 a_o}$$

and using the $\rho(z)$ dependence which corresponds to the present case.

The influence of external transverse fields $H_{x,y}$ can be described in analogy with the previous case. These fields could be produced for instance by currents in the coil connections and the field of the storage ring magnet.Substitution of

$$f_1(z) = -\omega \frac{H_y^o}{H_z} \quad , \quad f_2(z) = \omega \frac{H_x^o}{H_z} \ ,$$

into (3.10) yields

$$\frac{v_\perp}{v_{/\!/}} \lesssim \frac{(H_\perp)_{max}}{H_z} \tag{3.13}$$

To use (2.15-23) in the present case, it is necessary to substitute :

$$\frac{\pi a}{\lambda} \cdot \frac{\Delta H}{H} \rightarrow \frac{(H_{x,y}^o)_{max}}{H_z} \text{ or } \frac{(H_\perp^o)_{max}}{H_z} \text{ or } H_\perp^o = \sqrt{(H_x^o)^2 + (H_y^o)^2}$$

The expressions (3.12, 3.13) describe the bending of the beam as a whole, without addition of the transverse velocity spreads.

The displacement of the beam axis in the bending region is produced by the bending field errors, this is the well-known "centrifugal" drift. It follows from (3.9) that :

$$\Delta x \lesssim \frac{\rho}{\omega^2} (1 - \cos \omega\Delta) < \frac{\lambda^2}{2\pi^2 R_o} \quad , \tag{3.14}$$

$$\Delta y \lesssim -\frac{\rho}{\omega^2} (\omega\Delta - \sin \omega\Delta) < -\frac{\lambda \phi_o}{2\pi} \tag{3.15}$$

The last inequality in (3.14, 3.15) corresponds to the case $H_\rho = 0$.

§ 4. - The design of the longitudinal magnetic field in the electron cooling device

4.1 The coils and the magnetic shielding

The longitudinal magnetic field, which has a good enough homogeneity from the gun up to the collector, is being produced by five solenoids three of these are straight, the two others resemble a section of a toroidal solenoid with an average radius of curvature of 50 cm. The solenoids are surrounded by steel screens (thickness : 15 mm) to collect the magnetic flux on the outside. The screens also help to shape the magnetic field at the ends of the solenoids (see 4.5 below).

The coils are made of copper bars, with a cross-section of 20 x 14 mm^2; the bars have a central cylindrical hole (diameter : 10 mm) for the passage of cooling water. The pitch of the coil is d = 2.4 cm, the maximum current is 5 kA, the maximum magnetic field : 3 kG.

The return current from the solenoids to the generator is carried by three bars in parallel, located symetrically inside the shielding, in order not to saturate the shielding (Fig. 5). The transverse magnetic fields due to the currents in the parallel bars are minimized by the symmetrical arrangement. Clearly, if the total current was going through a single bar, the transverse field on the solenoid axis would be

$$H_{\perp} = \frac{d}{2\pi R_{sol}} H_o \quad ,$$

where d is the pitch of the spiral, R_{sol} the radius of the solenoid cross-section. If three bars are used and the currents are approximately equal, the transverse field will be much smaller :

$$\frac{H_{\perp}}{H_o} = \kappa \frac{d}{6\pi R_{sol}} \sqrt{\left(\frac{I_1-I_3}{I_3}\right)^2 + \left(\frac{I_2-I_3}{I_3}\right)^2 - \frac{(I_1-I_3)\,(I_2-I_3)}{I_3^{\,2}}} \qquad (4.2)$$

$$\kappa = \left(1 + 4\,\frac{R_{sol}^2}{L_{bar}^2}\right)^{-\frac{1}{2}}$$

The coefficient κ describes the effect of the finite length L of the bars. For the dimensions of the straight solenoids adopted in our device, the expressions (4.2, 4.3) give :

$$\frac{H_\perp}{H_o} \lesssim 2.10^{-2} \kappa \left(\frac{\Delta I_i}{I}\right)_{max} \qquad (4.4)$$

The transverse fields of the connection bars could, of course, also be compensated with correction coils.

The currents in the bars were adjusted by changing their resistivities. The equivalent circuit scheme is shown in Fig. 4. The calibration was made by measuring the voltage on the bars, at different points which are far enough away from each other.

The connecting bars in the bending region produce transverse fields, which are directed parallel to the bending axis. This arises from the fact that the ideal trajectory in the bending region is not located in the solenoid centre (Fig. 5).

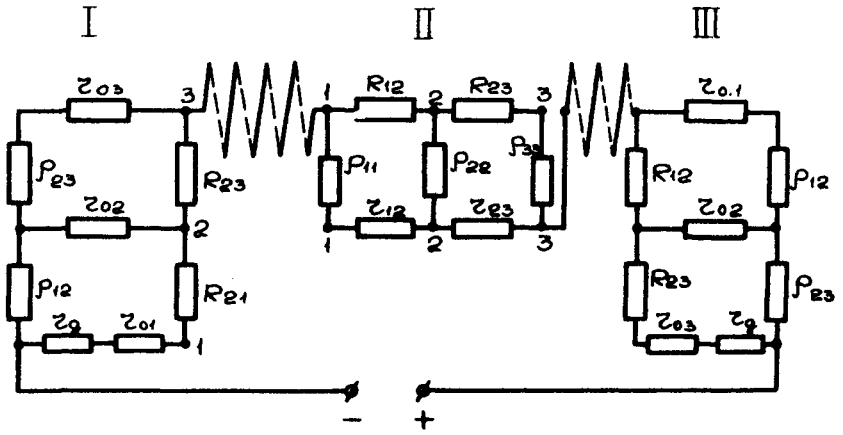

Fig. 4 : The scheme of the coil connection

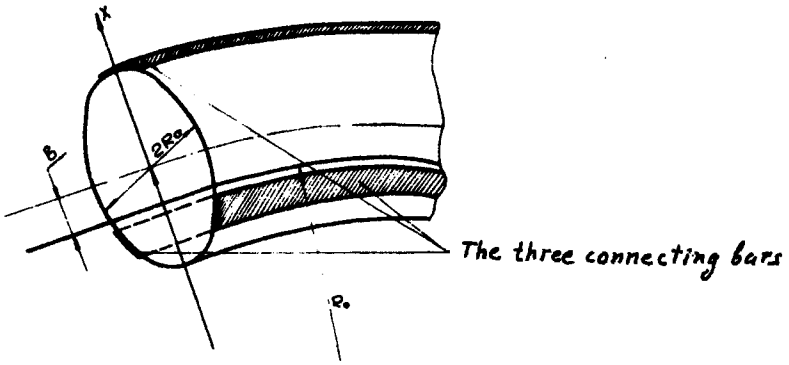

Fig. 5 : Co-ordinates used for the transverse fields in the bending region.

The field which is produced with three bars on the central trajectory is :

$$H_x = 0.6 \frac{b^2 d}{R_{sol}^3 + b^3} H_o \qquad (4.5)$$

where b is the trajectory displacement, R_{sol} the radius of the cross-section of the toroid, d the pitch of the solenoid spiral. In our case, $H_x/H_o \sim 2.10^{-3}$. This field increases or decreases the bending field, but the beam perturbation due to this field is negligible.

The standard Hall device was used for field measurements; three field components were measured. The measurement accuracy for transverse components was approximately 1 G, with the longitudinal field excited to 1 kG.

4.2 The straight section fields

The measurements of the transverse field components in the straight sections had given at first surprising results. It is known [IV-5] that the transverse field in a straight solenoid which is wound of a wire with

rectangular cross-section of width h and pitch d, is negligible near the axis :

$$\frac{H_{\perp}}{H_{//}} = \frac{\pi(d-h)}{h^{3/2}} \sqrt{R_{sol}}\; e^{-\frac{2\pi R_{sol}}{h}} \qquad (4.6)$$

However the measurements gave a value $H_{\perp}/H_{//}$ of the order of 10^{-2} (Fig. 6a). It is presently understood that the reason of this discrepancy was connected to a different skewness of the turns. The correction of these differences has given good results (Fig. 6b).

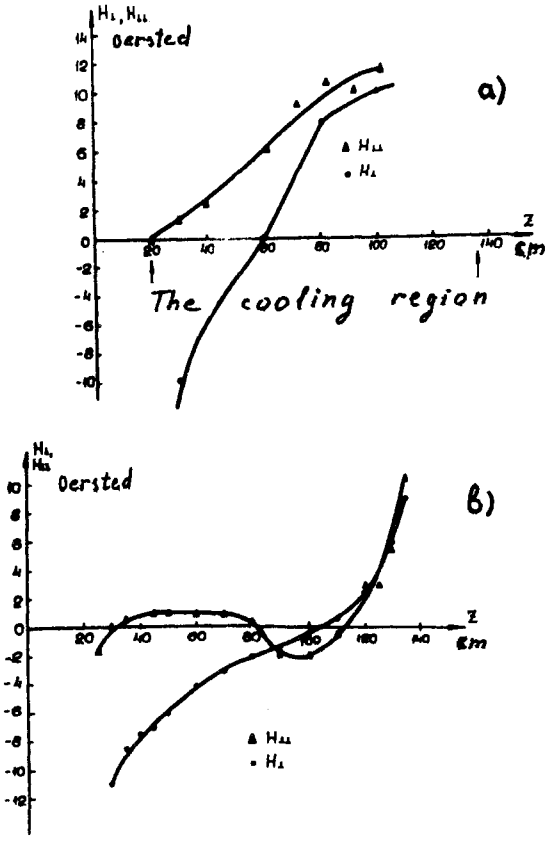

Fig. 6 : The transverse field components in the cooling region before (6a) and after coil correction. H_o = 1 kG (6b).

The next step in the field correction was made with special turns wound on the solenoid. The coil construction is shown in Fig. 7.

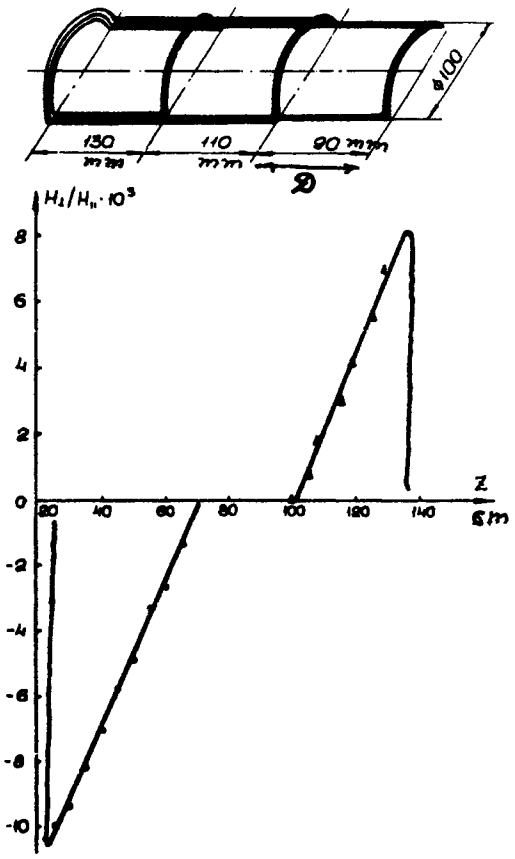

Fig. 7 : The correcting coils and their magnetic field

The linearly rising magnetic field is produced by n overlapping coils of different length. Each has N_i turns and the maximum field is

$$H_{\perp max} = \frac{8n\ N_i}{c\ D}\ I \qquad (4.7)$$

Here D is the difference in the length of the coils, nD the length of the transverse field region, I the current in the coils. The results of field corrections by use of these coils is shown in Fig. 8.

Other coils permit to produce a homogeneous transverse field along the whole cooling region.

4.3 The magnetic fields in the bending region

The main purpose of the magnetic field measurements in the bending region was to define the curvature radius of the longitudinal field lines. It was convenient to measure the field components along straight lines which are the continuation of the axis of the solenoid under consideration (Fig. 9). If one measures the field components, which lie in the plane AOB and are parallel ($H_{\perp}$) and perpendicular ($H_{//}$) to these straight lines (OA, OB) it is possible to find the curvature radius of the central field line $R_o(s)$ where s is the distance along the field line. In this case, the curvature radius, which crosses the straight line OA in the point s, is related to $R_o(s)$ by :

$$R(s) = \frac{R_o(s)}{\cos \theta} \quad , \quad \operatorname{tg} \theta = \frac{H^*_{\perp}}{H^*_{//}} \tag{4.8}$$

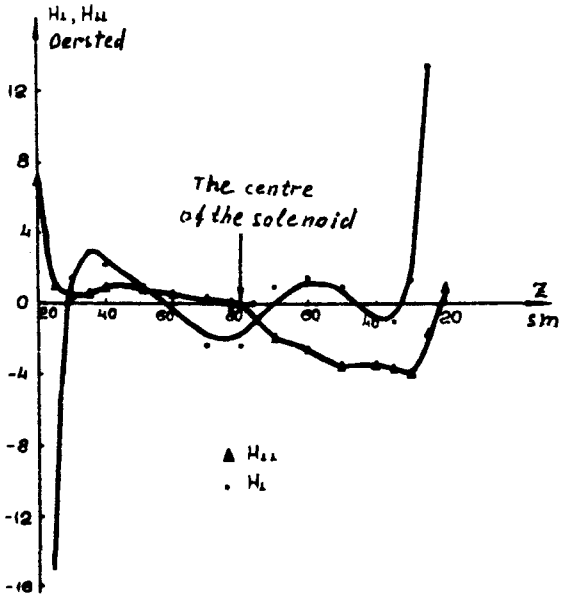

Fig. 8 : The transverse field in the cooling region after the use of the correcting coils. H_o = 1 kG

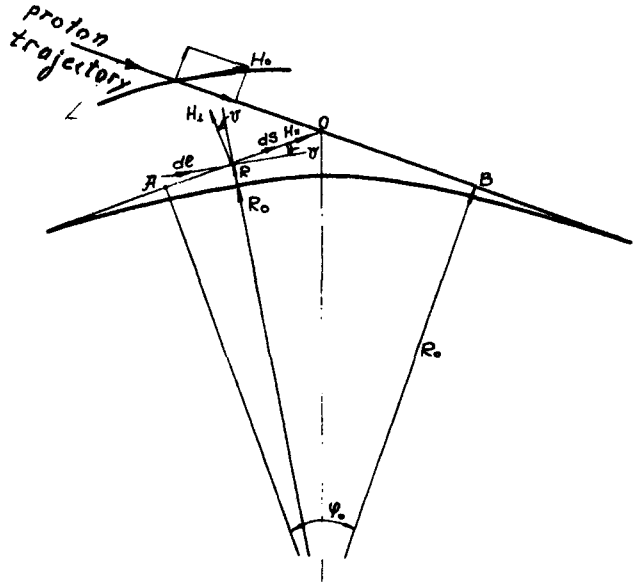

Fig. 9 : The field measurements in the bending region

The length element of the field line is :

$$d\ell = \frac{ds}{\cos\theta} \quad , \tag{4.9}$$

and it follows :

$$R_o(s) = R(s)\cos\theta = \frac{d\ell}{d\theta}\cos\theta = \frac{ds}{d(\mathrm{tg}\,\theta)} \tag{4.10}$$

The results of measurements are shown in Fig. 10 : R_o = const = 53 cm for

the part of the trajectory whose length is $\pm$ 10 cm.

To have the minimum beam perturbation in the bending region, it is necessary to produce the bending field

$$H_\rho(s) = R_o^{-1}(s) \tag{4.11}$$

The coils of the bending field have the simple design shown in Fig, 11. If the upper coil is not displaced with respect to the lower one, the field decreases linearly with the distance D (D is the width of the coils - see Fig. 11) and the field has decreased to half of the maximum field at the end of the coil. The displacement of the coils b permits to adjust the length of the field decreasing region.

The field and currents in the coils are described by equation (4.7), with n equal to 1.

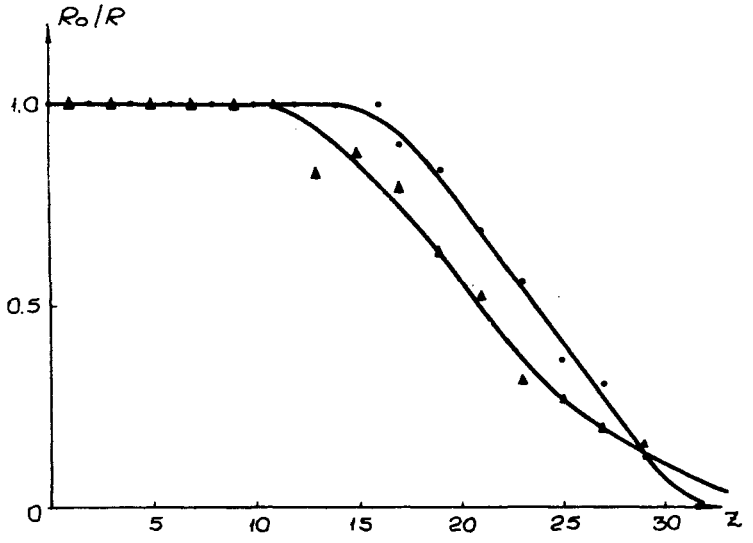

Fig. 10 : The curvature of the central trajectories in the first (●) and second (Δ) bending region.

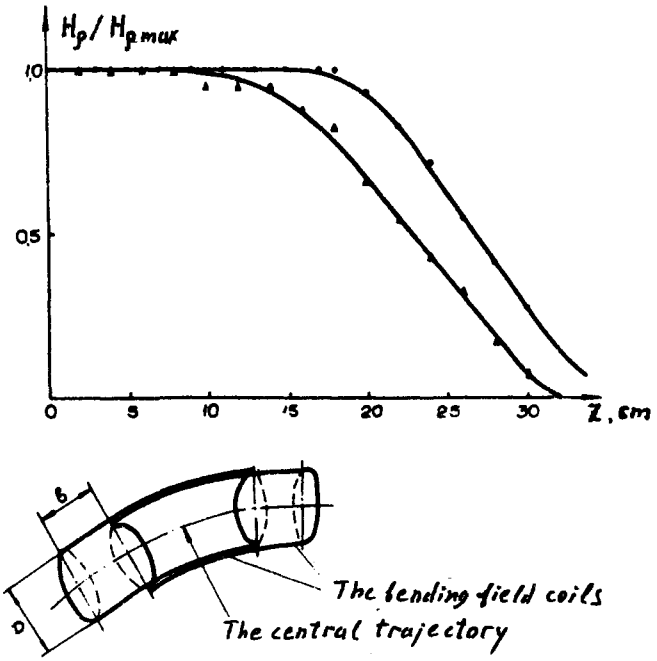

Fig. 11 : The bending field and the coils

4.4 The field at the ends of the solenoids

The proton beam needs to be guided into the cooling region. To get to this region it must necessarily pass through the solenoids. The simplest solution is to use the place where the toroidal solenoids meet with the straight solenoids, for entrance into the cooling region. But in this case one needs to combine two solenoids with unequal cross-sections. The difficulty is connected with the inhomogeneities of the magnetic field, at the junction of the two solenoids :

$$H_z = H_o \left\{ 1 + \frac{z}{2} \left(\frac{1}{\sqrt{R_{sol}^2 + z^2}} - \frac{1}{\sqrt{r_{sol}^2 + z^2}} \right) \right\} \qquad (4.12)$$

The z-coordinate is being measured here from the junction point (Fig. 12). The region of the field inhomogeneity has a length

$$\Delta \sim \frac{R_{sol}\, r_{sol}}{\sqrt{R_{sol}^2 + r_{sol}^2}} \qquad (4.13)$$

and the maximum field perturbation is

$$\frac{|\Delta H_z|}{H_z} \sim \frac{1}{2} \left| \frac{1}{\sqrt{2 + \left(\frac{r_{sol}}{R_{sol}}\right)^2}} - \frac{1}{\sqrt{2 + \left(\frac{R_{sol}}{r_{sol}}\right)^2}} \right| \qquad (4.14)$$

In our case ($r_{sol} \sim 10$ cm, $R_{sol} \sim 20$ cm) using (2.23d) and assuming the most favourable case of perturbation, we obtain $v_\perp / v_{//} \sim 3.10^{-2}$, which is much too high.

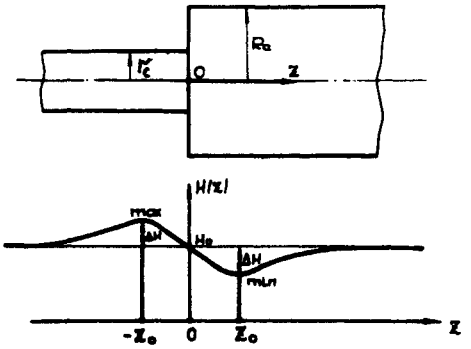

Fig. 12 : The distribution of the longitudinal magnetic field near the junction of two solenoids with different diameter without steel screens.

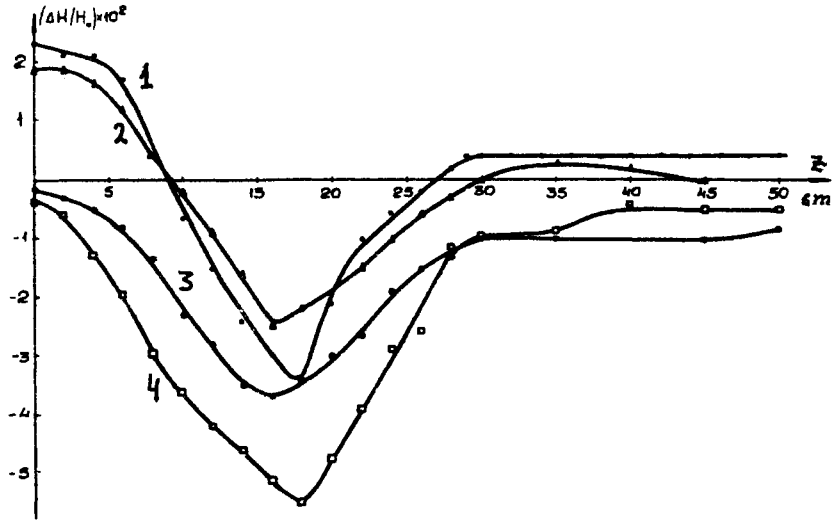

Fig. 13 : The distribution of the longitudinal magnetic field near the junction of the two solenoids with steel screens.

The co-ordinate z is measured from the centre of the bending region (point 0) along the line OA, OB (Fig. 9).

1,2 - the left "toroid", - 3,4 - the right "toroid" (see Fig. 1).

The inhomogeneity could be decreased by the use of magnetic screens. This method also solves the problem of joining two solenoids, with axes displaced with respect to each other. The results are illustrated in Fig. 13. The smallness of the field perturbation thus obtained guarantees that $v_\perp/v_{//} \lesssim 1.10^{-3}$.

To produce the homogeneous magnetic field in a short solenoid, it is possible to use a flat magnetic screen which is placed on the end of the solenoid and is connected (magnetically) to the external shield. The results are shown in Fig. 14.

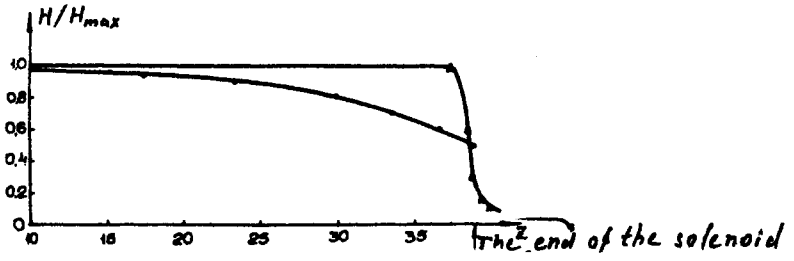

Fig. 14 The approximation to an "infinite" solenoid

● The calculated field near the end of the solenoid without screen

▲ The measured field with screen

The influence of the magnetic field ripple on the electron motion is very small. The possible effects, which have to be taken into account lead to the requirement that

$$\frac{\Delta H(t)}{H} \lesssim 10^{-3}$$, which is easy to obtain.

But there are some effects connected with the proton motion in the storage ring incorporating the cooling device (see § 9). The magnetic field fluctuations can produce "vibrations" of the closed proton orbit. In fact, in the experiments $H(t)/H$ was smaller than 1.10^{-3}.

§ 5. - The electron gun in the longitudinal magnetic field

To form the electron beam inside the longitudinal magnetic field, the most convenient method is to use an electron gun with a Pierce optics. But in this case it is necessary to solve the problem of the transition of the electron beam from the accelerating region to the subsequent channel. A possible solution is reported here.

5.1 The Pierce gun

The electric field inside the electron beam is flat, if a Pierce gun is used ; the radial field component is zero but the potential and the longitudinal component is rising in accordance with the well-known law

$$\begin{aligned} V(z) &= (\kappa j)^{2/3}\, z^{4/3} \equiv V_o \left(\frac{z}{d_o}\right)^{4/3} \\ E(z) &= \frac{4}{3}\,(\kappa j)^{2/3}\, z^{1/3} \qquad (5.1) \\ \kappa &= \frac{9\pi}{\sqrt{2}}\sqrt{\frac{m}{e}} = 4.35 \cdot 10^5\, V^{3/2} \cdot A^{-1} \end{aligned}$$

Here, d_o, V_o are the distance and potential difference between cathode and anode. When the beam current is limited by the space charge, these conditions are achieved by using special electrodes. The maximum of the electric field is located near the anode and has the value

$$E_{max} = \frac{4}{3} \cdot \frac{V_o}{d_o} \qquad (5.2)$$

From (5.1, 5.2) it follows that :

$$j \simeq \frac{9}{16} \cdot \frac{E_{max}^2}{\kappa \sqrt{V_o}} \qquad (5.3)$$

Therefore the maximum current density for $E_{max} \sim 50$ kV/cm and $V_o \sim 100$ kV is smaller than 10 A/cm^2.

5.2 The resonance optics

The exit from the accelerating region acts on the electrons like a defocusing lens. The focal length [IV-4] is ideally :

$$f \sim - \frac{2\beta^2\gamma mc^2}{e\, E_{max}} \sim - 3\, d_o \qquad (5.4)$$

In practice when the anode aperture has the same order of magnitude as the distance d_o, the focal length can be made about equal to d_o. In both cases, the defocusing effect is very strong and

$$\frac{v_\perp}{v_{//}} \sim \frac{a}{d_o} \sim 10^{-1} \qquad (5.5)$$

When the longitudinal magnetic field is used, it is possible to reduce the defocusing effect. For this purpose the region over which the accelerating field decreases to zero has to extend over a length $\propto \lambda$ (resonance optics). If we neglect the influence of the space charge in the gun exit region, we obtain from equations (2.1, 2.5, 2.6)

$$\frac{v_\perp}{v_{//}} \lesssim \frac{e}{\beta^2\gamma mc^2} \sqrt{\left[\int E_r \sin \omega(\chi - z)\, d\chi\right]^2 + \left[\int E_r \cos \omega(\chi - z)\, d\chi\right]^2} \qquad (5.6)$$

The integration has to be made through the exit region. The comparison of (5.6) and (2.12) shows that it is possible to use the results of (2.15-25), if we replace :

$$\frac{\Delta H}{H} \longrightarrow \frac{\lambda^2}{2\pi^2} \cdot \frac{e\, E_r}{a\beta^2\gamma mc^2} \qquad (5.7)$$

In particular, a suitable choice of the length of the exit region will lead to no perturbations of the electron beam.

The first possibility is to form in the exit region a linearly decreasing accelerating field that produces a constant transverse electric field E_r = const, and to choose the length of the exit region equal to an integer multiple of λ. This is the case of "resonance optics".

To form such a field, a gun was used with three anodes with

potentials properly chosen to provide a slowly changing (almost constant) transverse field E_r in the exit region. The results of model measurements are shown in Fig. 15.

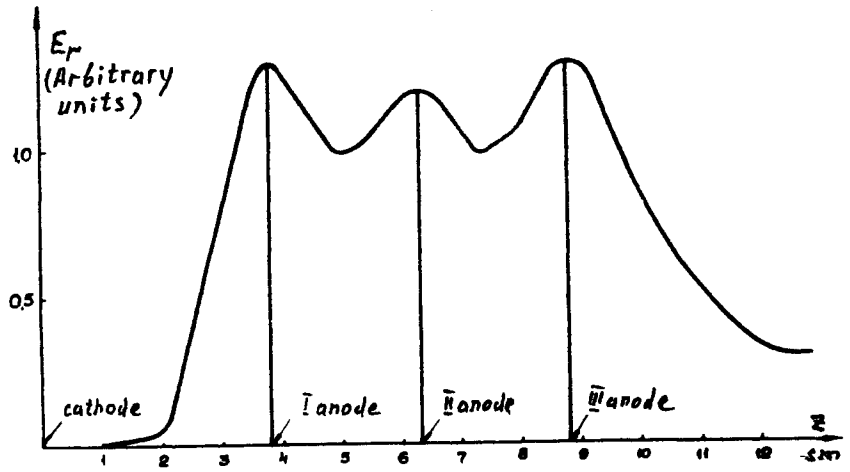

Fig. 15 : The distribution of the radial component of the electric field in the exit region of the electron gun

The results of experiments with our electron gun, which are in good agreement with the considerations discussed above, are described in detail in Ref. II-5.

---

* A comment during translation

The requirements for the accuracy of position and shape of the Pierce electrodes are not very stringent. As was shown by computer calculations and confirmed in our cooling experiments, it is possible to obtain a good cooling with a gun which has a flat cathode electrode.

5.3 The adiabatic optics

A variant of the resonance optics uses a transverse electric field in the exit region which varies slowly, so that:

$$\frac{dE_r}{dz} \lesssim \frac{E_r}{\lambda} \tag{5.8}$$

In this case, the conditions of the adiabatic motion are satisfied and the perturbations due to transverse fields are negligible. To achieve this situation, one can make the anode aperture larger than the beam diameter.

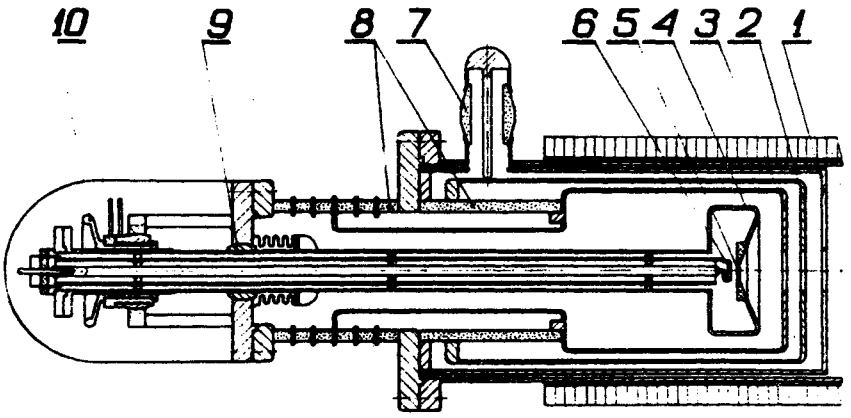

Fig. 16 : The electron gun

1-2-3 : anodes; 4 : Pierce electrode (the cathode potential); 5 : main cathode; 6 : heating cathode (for an auxiliary electron beam used to heat the main cathode); 7,8 : insulators; 9,10 : the adjustment mechanism

6. - The Collector for Electron Energy Recovery

The electrons leave the cooling region practically without energy losses, and energy recovery can be very effectively used in electron cooling devices. In this case, the electron device "stores" the reactive power

$$P_r = I V_o$$

and only the active power

$$P_a = \Delta I \cdot V_o + I V_{col} \tag{6.1}$$

has to be supplied by the power supply. Here V_o is the cathode potential, V_{col} is the potential difference between cathode and collector, I the beam current, ΔI the current losses, which are mainly determined by the current of secondary (untrapped) electrons in the collector. The maximum current that can be trapped in the collector is determined by the potential difference between cathode and collector; it is the same current limit which was noted in § 1. For non relativistic energy, the expression (1.18) can be written as

$$I_{lim} = \sqrt{\frac{e}{m}} \left(\frac{2}{3} U_{col}\right)^{3/2} \frac{1}{1+2\ell n \frac{\rho}{a}} \simeq 25.4\ 10^{-6} \frac{U_{col}^{3/2}}{1+2\ell n \frac{\rho}{a}} \quad A\ V.^{-3/2} \tag{6.2}$$

For $\rho/a \sim 1$ and $V_{col} = 1$ kV this current limit is approximately 1 A.

The collector was designed using the experience of the experimental study which was performed on a special installation [II-1,3,6]. A detailed description of the study and the results is given in report [II-6].

The collector of our electron cooling device has the inner copper cylinder (Fig. 17) cooled with water (see later), the iron screen and the electrostatic screen at the collector entrance formed like a Pierce electrode. The aperture of the collector is 16 mm. The anode of the recovering region has an aperture of 30 mm.

To collect the magnetic flux, an external iron screen is used

in the collector too (Fig. 17). It is located inside the vacuum chamber, close to the collector.

The energy recovery was achieved with very high efficiency :

$\Delta I/I \leq 10^{-4}$, $V_{col} \simeq 1.5$ kV , $I = 1$ A

These results are mainly due to the use of magnetic field screeening in the collector and the electrostatic trap at the collector entrance [see II-6].

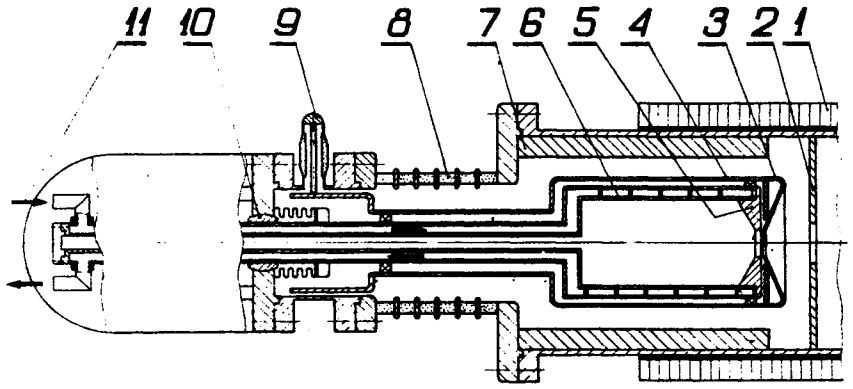

Fig. 17 : The collector

1 : solenoid; 2 : anode; 3 : electrostatic screen; 4 : the thin iron screen; 5,6 : cooled copper cylinder; 7 : the thick iron screen; 8 : insulator; 9 : the feedthrough for the electrostatic screen potential; 10 : adjustment mechanism; 11 : waterguide.

---

* Comments during translation

Some modifications of the collector were made later on [I-7] : two anodes were added, the anode aperture was increased to 40 mm, the collector aperture was enlarged to 30 mm, but, due to the use of additional electrostatic screens, the efficiency of the trap did not decrease and the collector efficiency is as high as before.

To reduce electric losses through the waterguide, three cooling loops are used : raw water (earth potential), oil, and a closed water loop (collector potential).

There were some difficulties during the first operation of the electron device. These difficulties are connected with gas evaporation from the walls in the presence of the electron beam. As a result, the beam current can be increased only very slowly, to allow the necessary pumping in the collector region. This can try the patience and optimism of the experimenters! If the vacuum chamber of the electron device can be baked, these difficulties are much smaller.

§ 7.- The assembly and adjustment

The electron device was assembled with high accuracy. Special attention was given to the gun assembly : the parallel alignment of the anodes, the orthogonality between cathode plane and gun axis and so on.

During the assembly of the solenoids, the position of the axes and the angles between axes were measured and corrected to high precision (to 0.1 mm and 1 mrad).

§ 8. - The Experiments with a Pencil Beam

To test the quality of the electron optics, the method of pencil beam tracking was used. To obtain a pencil beam, a screen with three holes (diameter : $\sim$ .2 mm) was placed on the cathode emitting surface; three thin beams were thus traced along the cooling region. To observe the beam position, a luminescent screen was used. This screen was moved along the cooling section and observed with a special optical telescope which is used in industry for precise alignment measurements. The position of the beam image was measured with an accuracy of approximately 0.1 mm (the centre of image). The holes on the cathode were located in the following way : the first one on the axis, the two others at a distance of 2 mm and 4 mm from the axis.

Three kinds of measurements were made.

8.1 The measurements of straightness of magnetic field lines

The electrons have in these measurements an energy of approximately 1 keV which is determined by the minimum screen luminosity. The results of measurements with "pencil" beams confirmed the first measurements which were made with the Hall measuring device (see Fig. 8), and only "pencil" beam measurements were later on used for field control.

8.2 The measurements of transverse electron velocities

These measurements were made with electrons which had the working energy of our cooling experiment, approximately 50 keV. By following the image position on the luminescent screen during magnetic field variations, it is possible to find the Larmor radius for transverse electron motion and, consequently, the transverse velocity :

$$\frac{v_\perp}{v_{//}} = \omega\rho_{\text{Larmor}} \sim 2\pi \frac{|\vec{\Delta r}|}{\lambda(H_1) + \lambda(H_2)} \qquad (8.1)$$

where $\lambda_{1,2}$ is the length of the Larmor period for the field strength, for which the beam images are focused, $|\vec{\Delta r}|$ the distance on the screen between these two points. It was possible to measure with an accuracy $v_\perp/v_{//} \sim (3 \div 5)\ 10^{-3}$.

8.3 The experimental measurements of H_ρ

It is necessary to achieve values of H_ρ as close as possible to the theoretical value for the smallest transverse energy. The error of H_ρ gives a beam displacement

$$\Delta y_1 = \frac{\lambda_1 \phi_o}{2\pi} \cdot \left(\frac{\Delta H_\rho}{H_\rho}\right)_1 \tag{8.2}$$

The displacement Δy_1 necessary to locate the "point beam" at the working energy onto the same point of the screen as the low energy beam corresponds to the H_ρ error

$$\Delta y_1 = \frac{\lambda_2 \phi_o}{2\pi} \cdot \left(\frac{\Delta H_\rho}{H_\rho}\right)_1 \tag{8.3}$$

Consequently,

$$\left(\frac{\Delta H_\rho}{H_\rho}\right)_2 = \frac{\lambda_1}{\lambda_2} \left(\frac{\Delta H_\rho}{H_\rho}\right)_1 \tag{8.4}$$

and the transverse velocity error is

$$\frac{v_\perp}{v_{//}} \lesssim \frac{\lambda_2}{\pi R_o} \left[\frac{\lambda_1}{\lambda_2} \left(\frac{\Delta H_\rho}{H_\rho}\right)_1\right] = \frac{\lambda_1}{\pi R_o} \left(\frac{\Delta H_\rho}{H_\rho}\right)_1 \quad . \tag{8.5}$$

For example, taking :

$$W_1 = 2 \text{ keV}, \ (\Delta H_\rho / H_\rho) = 0.2, \ H_o = 1 \text{ kG}, \ \lambda_1 = 1 \text{ cm},$$

the transverse velocity error is

$$v_\perp / v_{//} \lesssim 5.10^{-4} \quad .$$

In reality, the error is even smaller because the function $\Delta H_\rho(\phi)$ changes rather slowly.

§ 9.- The influence of the magnetic field in the electron device on the particle motion in the storage ring

The magnetic field of the electron device produces perturbations of the heavy particle motion :

1) Q-shifts,

2) coupling of vertical and horizontal betatron oscillations,

3) closed orbit deformations.

The first two effects are well known for storage rings, which have a longitudinal magnetic field in detectors, and antidotes are established. The order of magnitude of the first effect can be estimated, using :

$$\Delta Q \sim \frac{\beta}{f} \tag{9.1}$$

where

$$f \simeq \left(\frac{2p_m c}{eH}\right)^2 \frac{1}{L} \tag{9.2}$$

p_m is the heavy particle momentum, L the length of the longitudinal field region and β the focusing function of the storage ring in this region.

The closed orbit deformation takes place due to the influence of the components of the magnetic field perpendicular to the heavy particle motion. It is easy to calculate the total bending angle which the heavy particles receive in the toroidal field region :

$$\left|\frac{dx}{ds}\right| = \frac{e}{P_m c} \int H_z \, ds = \frac{e\, H_o\, R_o}{p_m c} \left|\ell n \cos \phi_o\right| \tag{9.3}$$

The symbols used here are : H_o the strength of the longitudinal magnetic field of the electron device, R_o the curvature radius of the toroidal field region, ϕ_o its azimuthal length (electron bending angle), x horizontal coordinate for the storage ring, s the longitudinal one.

The displacement of the heavy particle trajectory is :

$$|\Delta x| = \frac{e\, H_o\, R_o^2}{P_m c} \left|\phi_o - \operatorname{tg} \phi_o\right| \tag{9.4}$$

The resulting motion and two different correction methods are schematically shown in Fig. 18.

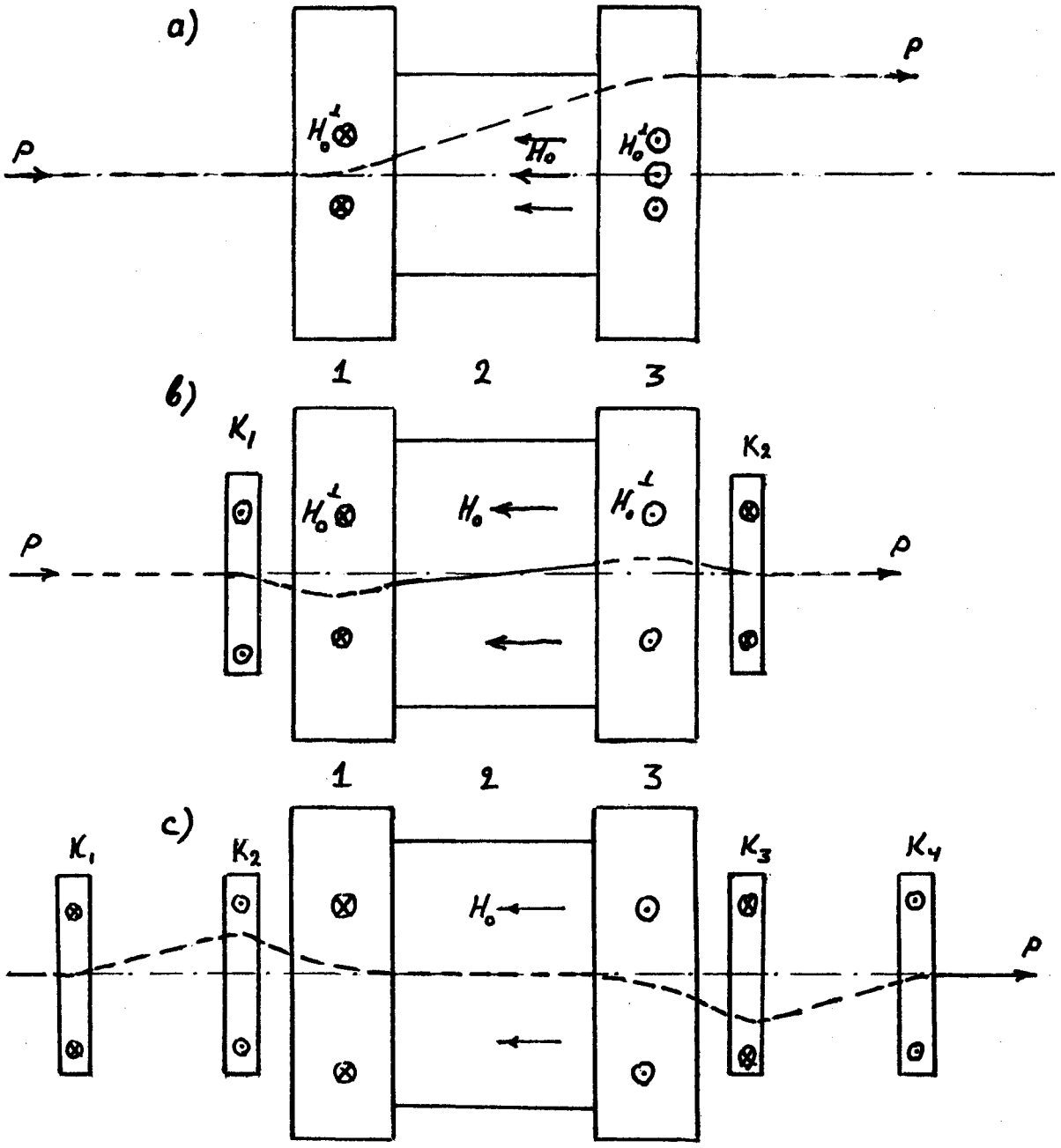

Fig. 18 : The influence of the magnetic field of the electron device on the closed orbit in the storage ring

a) the displacement of trajectory due to one passage
b) a simple correction scheme : in the cooling region, $\Delta x = 0$, $(dx/ds) \neq 0$;
c) a different correction scheme : in the cooling region $\Delta x = 0$, $(dx/ds)=0$;
1,3 : the toroidal field region; 2 : cooling region; $K_{1 \div 4}$: correction coils.

PART C

BIBLIOGRAPHY

I. Electron cooling - theory and experiments

I-1 G.I. Budker, Atomnaya Energiya, 22, 346 (1967).

I-2 Ya.S. Derbenev, A.N. Skrinsky, The kinetics of electron cooling of beams in heavy particle storage devices, Preprint INP 225, Novosibirsk, 1968; CERN Trans. 69-18; Particle Accelerators 1977 (being published).

I-3 "Proton-antiproton colliding beams", VAPP-NAP Group report in Proc. 8th Int. Conf. on High Energy Accelerators, CERN, 1971, p. 72.

I-4 G.I. Budker, N.S. Dikansky, V.I. Kudelainen, I.N. Meshkov, V.V. Parkhomchuk, D.V. Pestrikov, A.N. Skrinsky and B.N. Sukhina, Proc. 4th USSR National Conf. on Particle Accelerators, Vol. II, Moscow 1975, p. 309.

I-5 G.I. Budker, Ya.S. Derbenev, N.S. Dikansky, V.I. Kudelainen, I.N. Meshkov, V.V. Parkhomchunk, B.N. Sukhina, D.V. Pestrikov and A.N. Skrinsky, IEEE Trans. Nucl. Sci. NS-20, No. 5, 2093 (1975); Atomnaya Energiya 40, No. 1 (1976).

I-6 G.I. Budker, N.S. Dikansky, V.I. Kudelainen, I.N. Meshkov, V.V. Parkhomchuk, D.V. Pestrikov, A.N. Skrinsky and B.N. Sukhina, Particle Accelerators, Vol. 7, No. 4 (1976).

I-7 G.I. Budker, A.F. Buluchev, N.S. Dikansky, V.I. Kononov, V.I. Kudelainen, I.N. Meshkov, V.V. Parkhomchuk, D.V. Pestrikov, A.N. Skrinsky and B.N. Sukhina, New experimental results of electron cooling, Report to the Vth USSR National Conf. on Particle Accelerators, Dubna, 1976, Preprint INP 76-32 (Translated at CERN by O. Barbalat: PS/DL Note 76-25).

I-8 G.I. Budker, T.A. Vsevoloshskaya, N.S. Dikansky, I.N. Meshkov, V.V. Parkhomchuk, G.I. Silvestrov, A.N. Skrinsky, The proposal of Proton-Antiproton colliding beams with electron cooling in the "Big-Serpukhov Project", Report to the Vth USSR National Conf. on Particle Accelerators, Dubna, 1976, Preprint INP 76-73, Novosibirsk, 1976, (CERN translation by O. Barbalat in preparation).

I-9 Electron cooling and new possibilities in elementary particle physics, Report of VAPP-NAP Group to the Intern. Conf. on High Energy Particles Physics, Tbilissi, 1976 (in English).

I-10 Research and development of particle beam cooling techniques and a feasibility study of proton-antiproton colliding beam facility, ("Batavia-Project", 1976).

I-11 F. Bonaudi, S. van der Meer, B. Pope, Antiprotons in the SPS, CERN/DG-2, 11 January 1977.

I-12 N.S. Dikansky, V.V. Parkhomchuk, D.V. Pestrikov, Sov. Techn. Phys., (Transl. of V. 46, N 12, 1976).

I-13 N.S. Dikansky, D.V. Pestrikov, The coherent interaction between proton beam and cooling electron beam, Report to the Vth USSR National Conf. on Particle Accelerators, Dubna, 1976 (will also be published in Particle Accelerators).

I-14 Y.S. Derbenev, A.N. Skrinsky, The magnetized electron beam effects in electron cooling, Particle Accelerators (1977) (to be published).

II. Electron beam problems

II-1 A.I. Arenshtam, G.I. Budker, I.N. Meshkov, V.G. Ponomarenko, A.N. Skrinsky, Proc. of I USSR National Conf. on Particle Accelerators, II, 1970, p. 400.

II-2 V.I. Kudelainen, I.N. Meshkov, R.A. Salimov, The electron beam device for heavy particle cooling experiments, Preprint INP 72-70, Novosibirsk, 1970 (This publication, Part B).

II-3 A.I. Arenshtam, I.N. Meshkov, V.G. Ponomarenko, R.A. Salimov, A.N. Skrinsky, B.M. Smirnov, V.G. Fainstain, Journ. of Tech. Phys., (USSR), 41, N2 (1971).

II-4 G.I. Budker, V.I. Kudelainen, I.N. Meshkov, V.G. Ponomarenko, S.G. Popov, R.A. Salimov, A.N. Skrinsky and B.M. Smirnov, Proc. 2nd USSR National Conf. on Particle Accelerators, I, 1972, p. 31.

II-5 V.I. Kudelainen, I.N. Meshkov and R.A. Salimov, Journ. of Techn. Phys. (USSR), 11, 2294 (1971).

II-6 V.I. Kudelainen, I.N. Meshkov, V.V. Parkhomchuk, R.A. Salimov, A.N. Skrinsky, V.G. Vainstein, Journ. of Techn. Phys. (USSR), 46, N8, 1678 (1976).

II-7 V.P. Ginkin, I.N. Meshkov, A.N. Skrinsky, V.G. Fainstain, Instruments and Experimental Techniques, V 15, N6, Part. I, 1642 (1972).

III. NAP-M - proton storage ring for electron cooling experiments

III-1 V.V. Anashin, G.I. Budker, N.S. Dikansky, V.I. Kudelainen, A.S. Medvedko, I.N. Meshkov, Y.V. Parkhomchuk, D.V. Pestrikov, V.G. Ponomarenko, R.A. Salimov, A.N. Skrinsky and B.N. Sukhina, Proc. of 4th USSR National Conference on Particle Accelerators II, 1975, p. 304.

III-2 V.V. Anashin, G.I. Budker, A.F. Bulushev et al, Storage ring NAP-M I. The magnets and vacuum system" Instr. and Exp. Techn. N4 (1976), Novosibirsk preprint.

III-3 B.A. Baklakov, V.M. Borovikov et al, Storage ring NAP-M. II. The magnet current stabilization", Instr. and Exp. Techn. N4 (1976).

III-4 V.F. Veremeenko, N.S. Dikansky et al, "Storage ring NAP-M. III. Acceleration equipment - beam control system", Instr. and Exp. Techn. N4 (1976).

III-5 Yu.A. Bolvanov, V.I. Kononov et al, "Storage ring NAP-M. IV. "The system of operation with storage ring", Instr. and Exp. Techn. NY (1976), Novosibirsk preprint.

IV. Related references

IV-1 I.M. Kapchinsky, Particle dynamics in linear accelerators, Moscow, 1966.

IV-2 M.V. Nezlin, M.I. Taktakishvili, B.S. Trubnikov, JETP 55, (1968).

IV-3 A.A. Kolomensky, A.N. Lebedev, Theory of cyclic accelerators, Moscow, Fizmatizdat, 1962.

IV-4 P.A. Sturrock, Static and dynamic electron optics, Cambridge University Press, 1955.

IV-5 H. Buchholz, Calculations of electric and magnetic fields, Springer, Berlin, 1957 (in German).

IV-6 S.T. Beljaev, Manual, Plasma physics and the problem of controlled thermonuclear reactions, Vol. 3, p. 66, Moscow, 1958.